CMB Lecture

Petnica Summer Institute 2024

Enea Di Dio

Outline

1. What is the CMB? (hot big bang and thermal history)
2. CMB statistics
3. Light propagation
4. Initial conditions
5. Plasma evolution (transfer function)
6. Cosmological Parameters

The expanding Universe

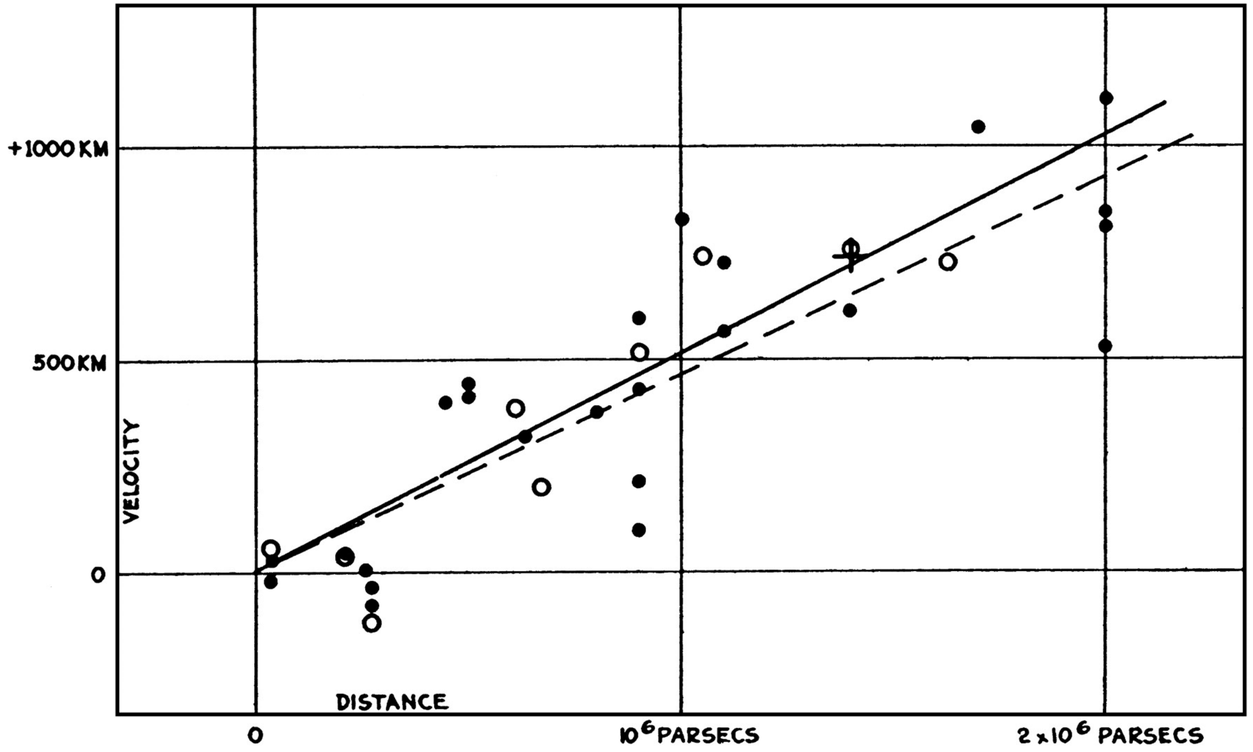

Hubble 1929

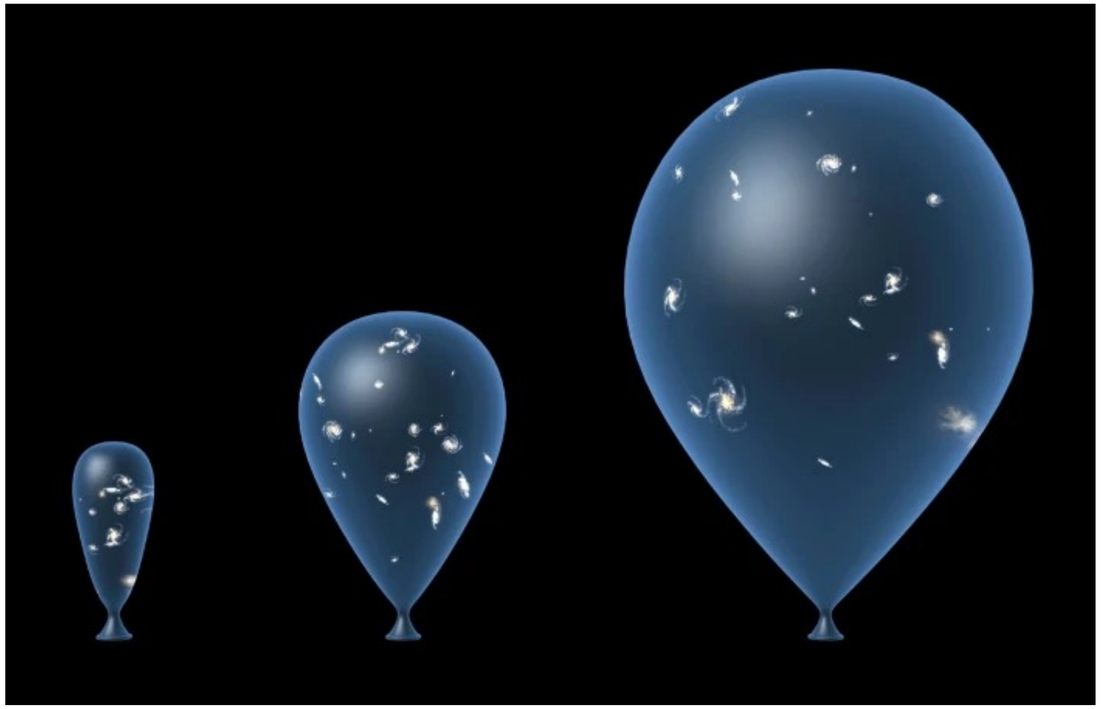

The farther away a galaxy is, the faster it appears to be receding from our position

Copernical Principle

The universe is expanding

The expanding Universe

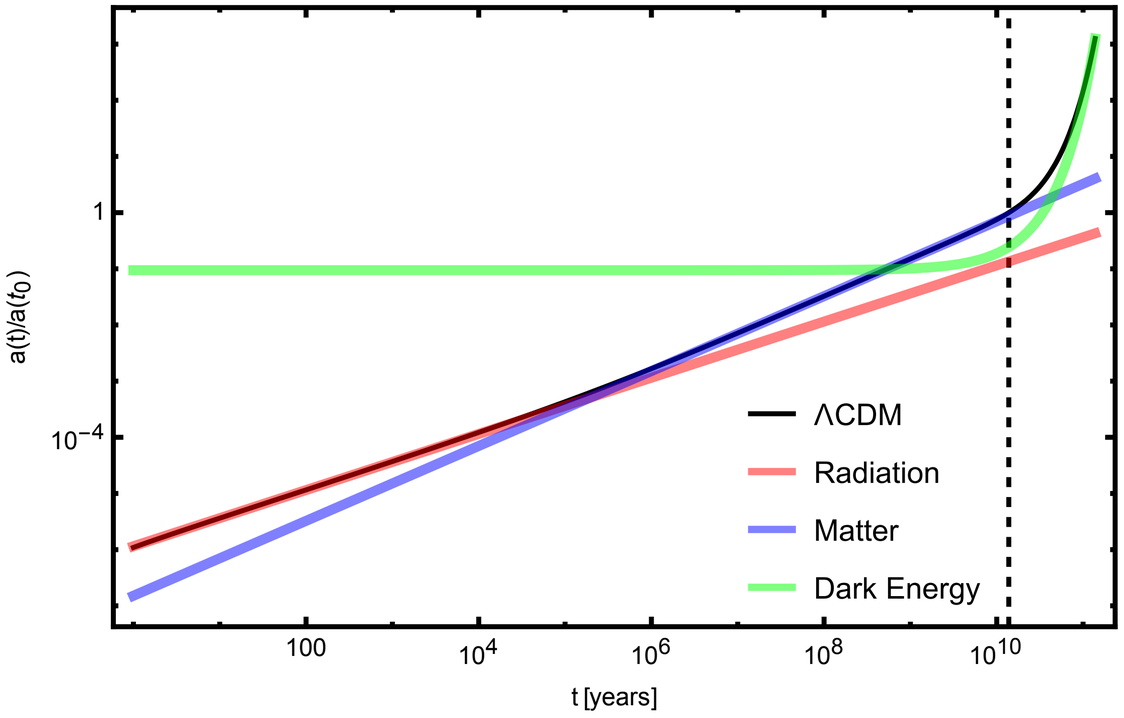

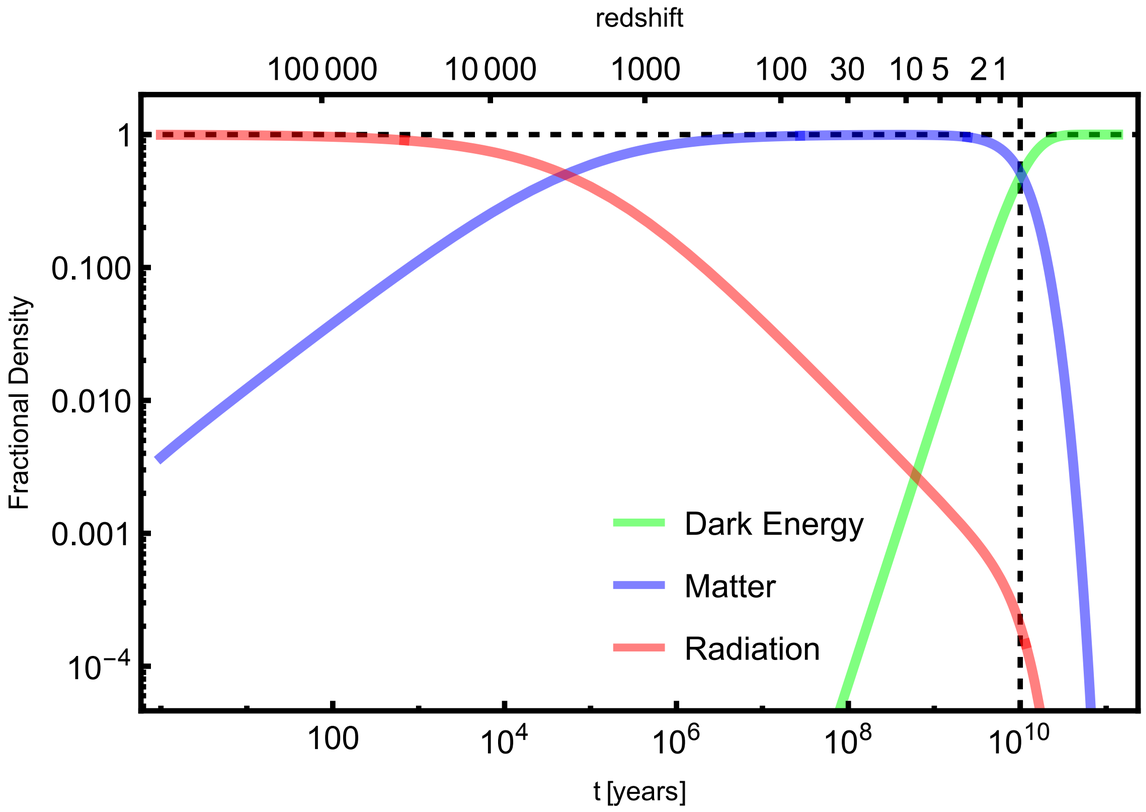

The expanding Universe

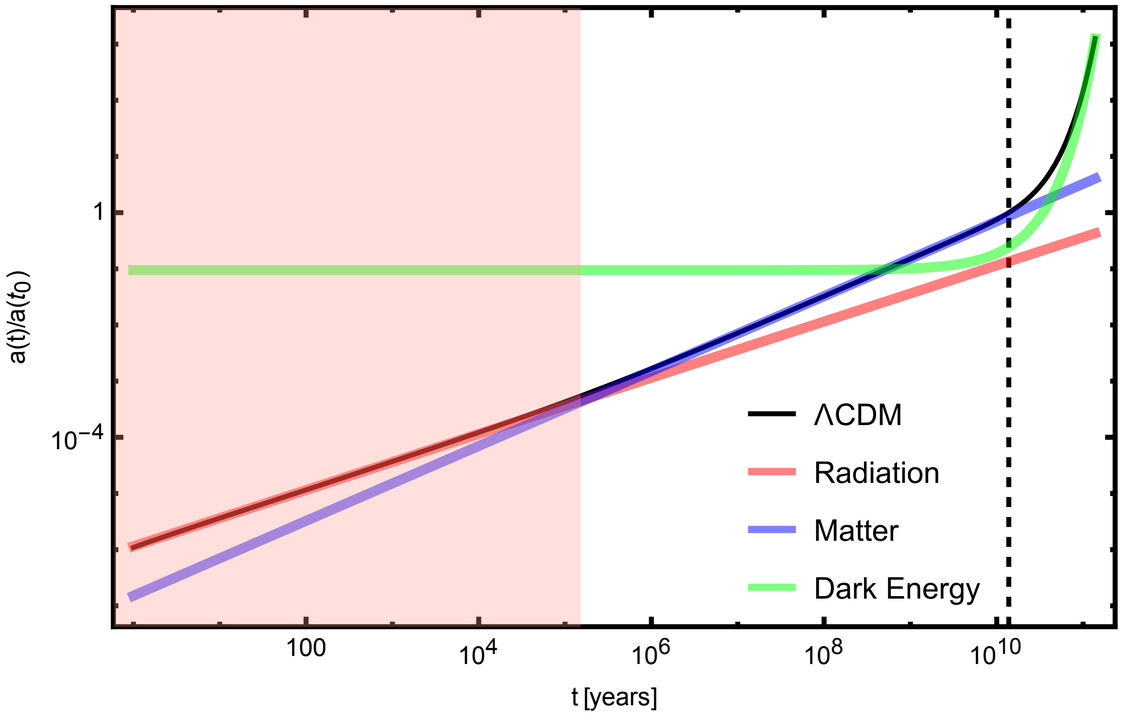

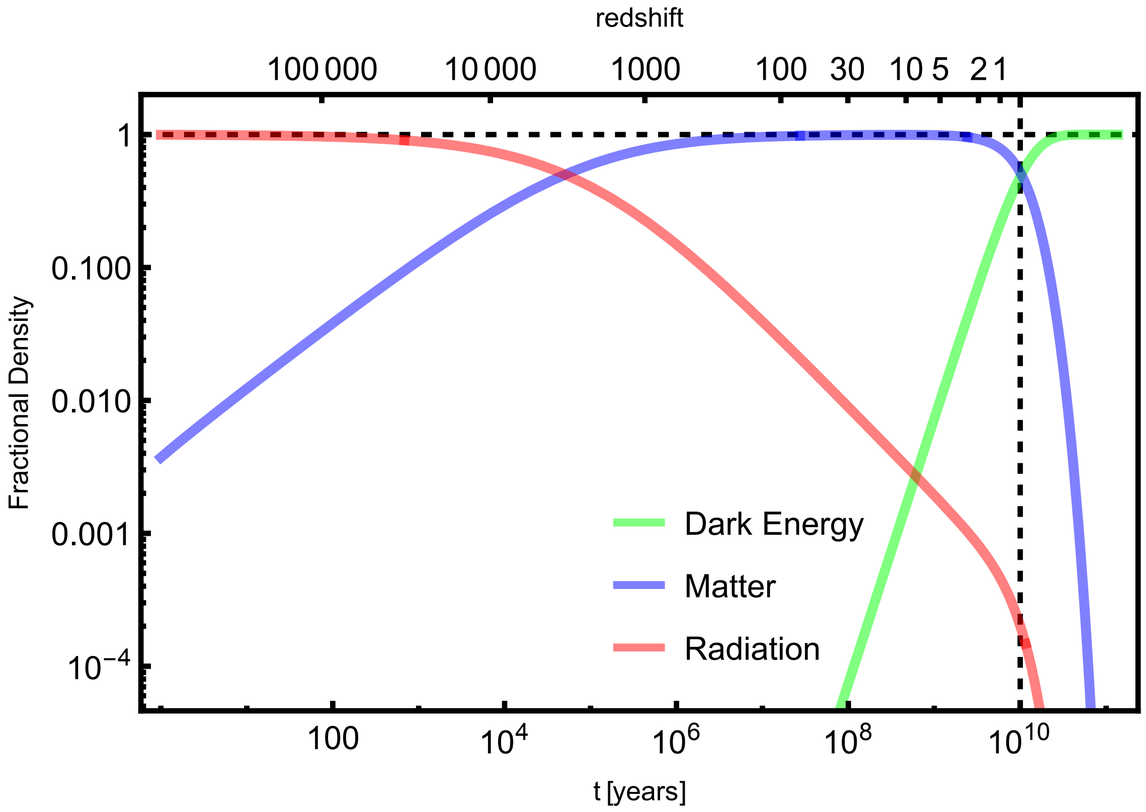

The expanding Universe

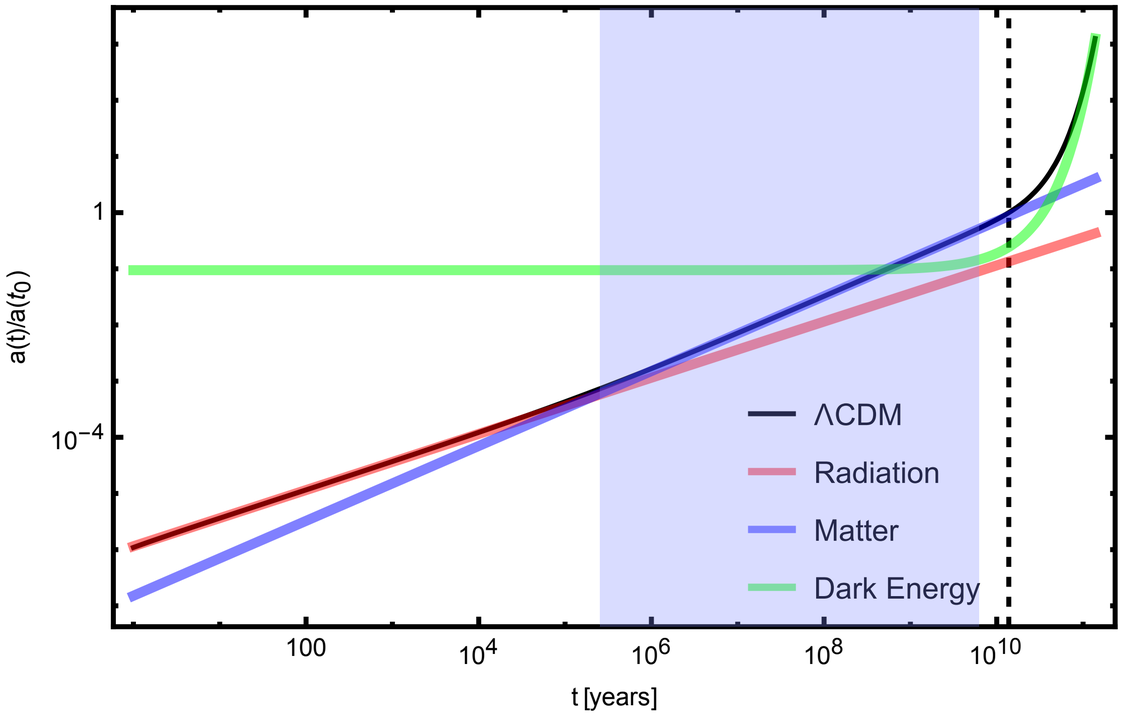

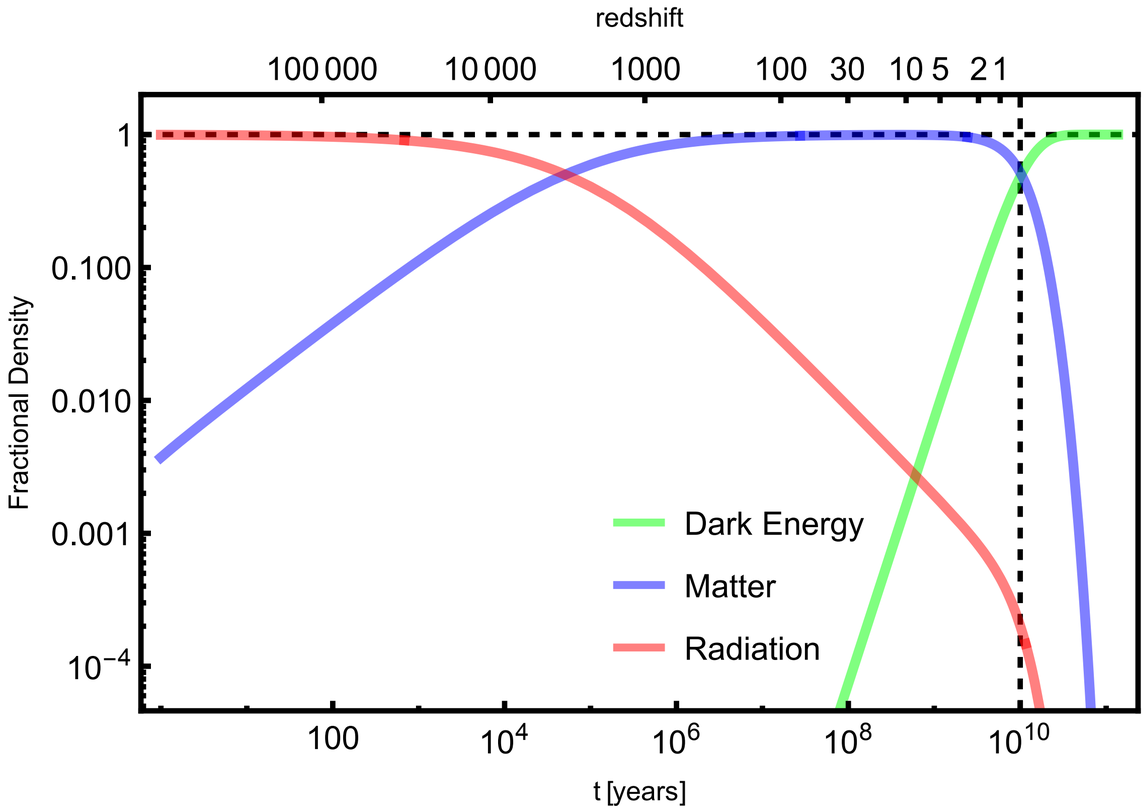

The expanding Universe

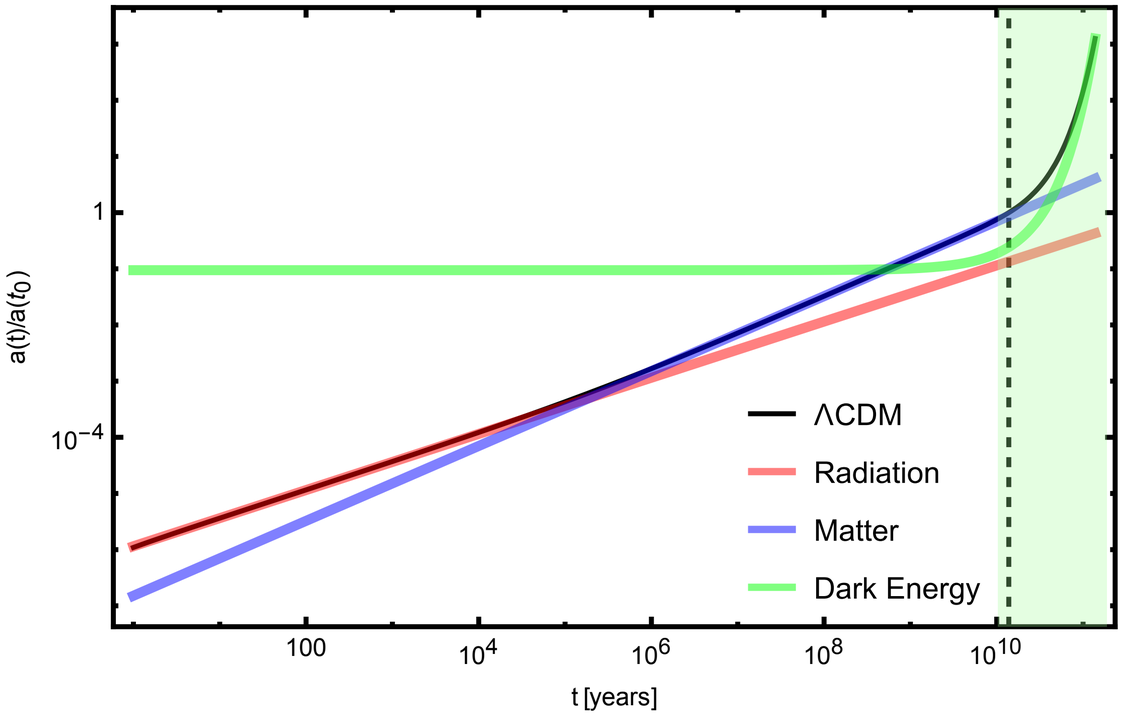

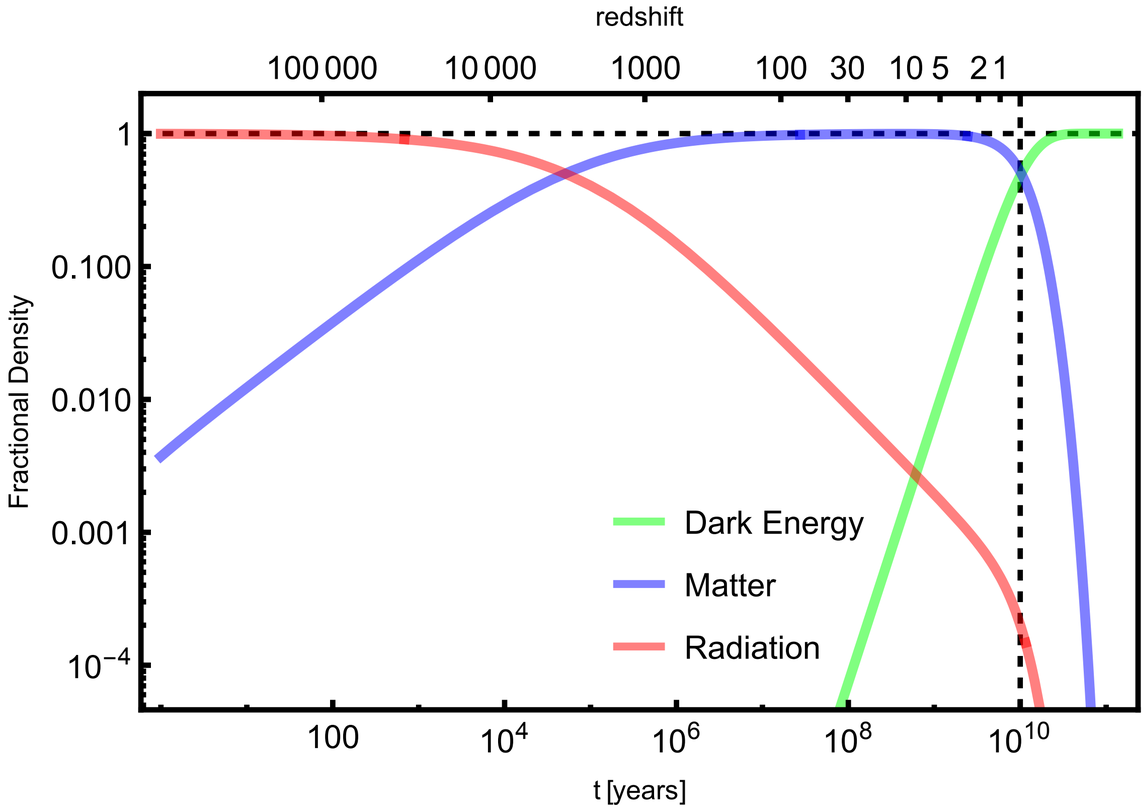

The expanding Universe

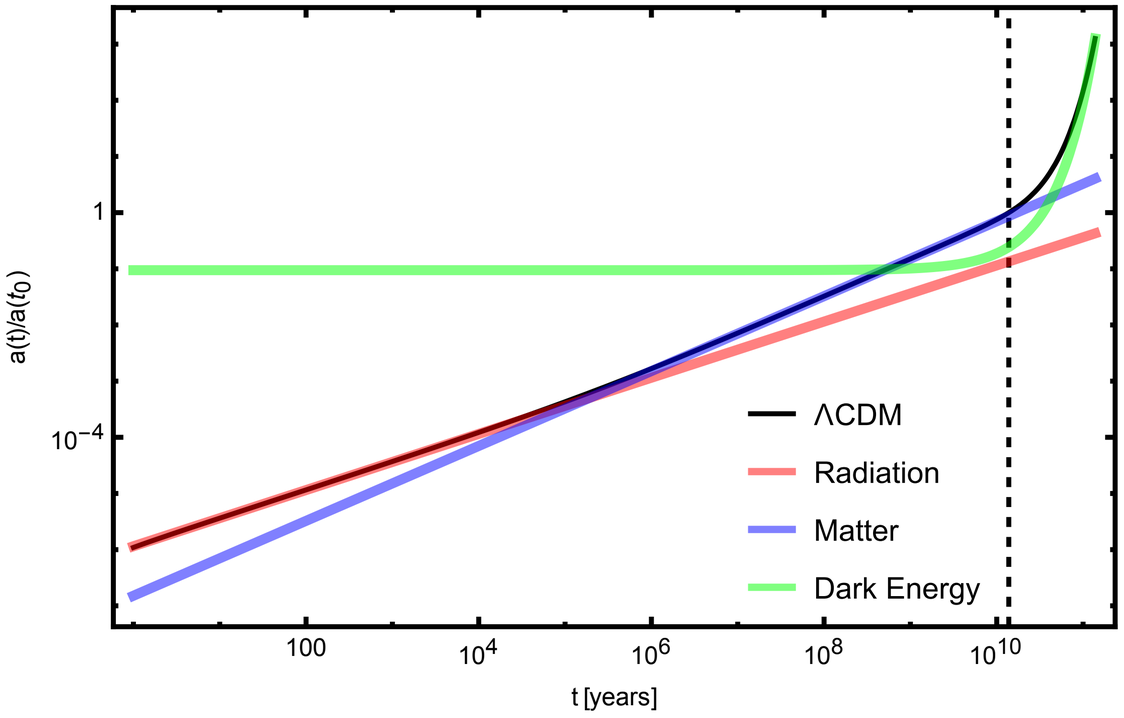

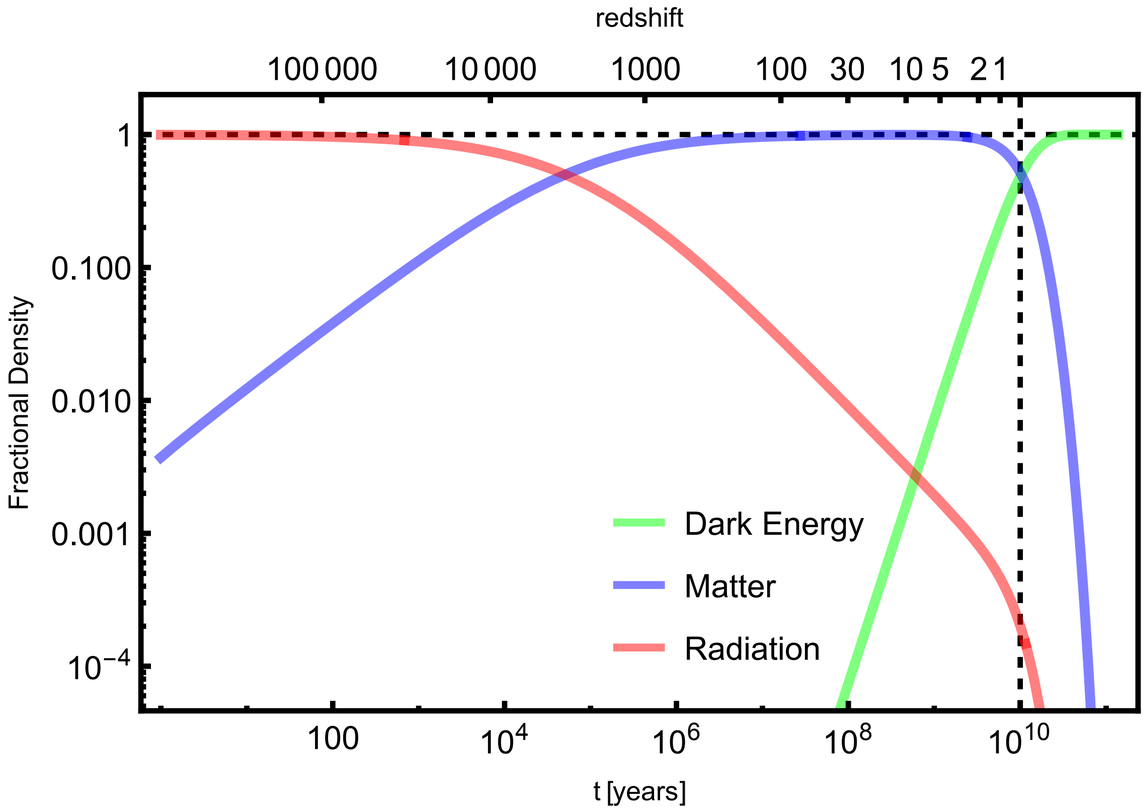

The expanding Universe

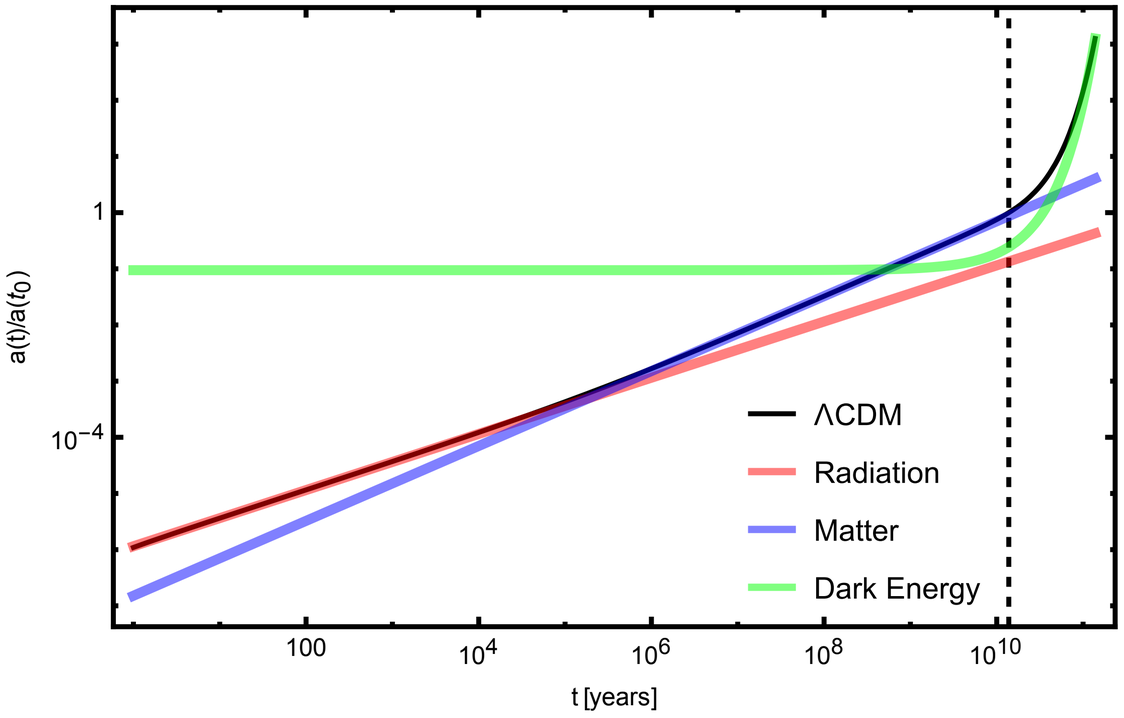

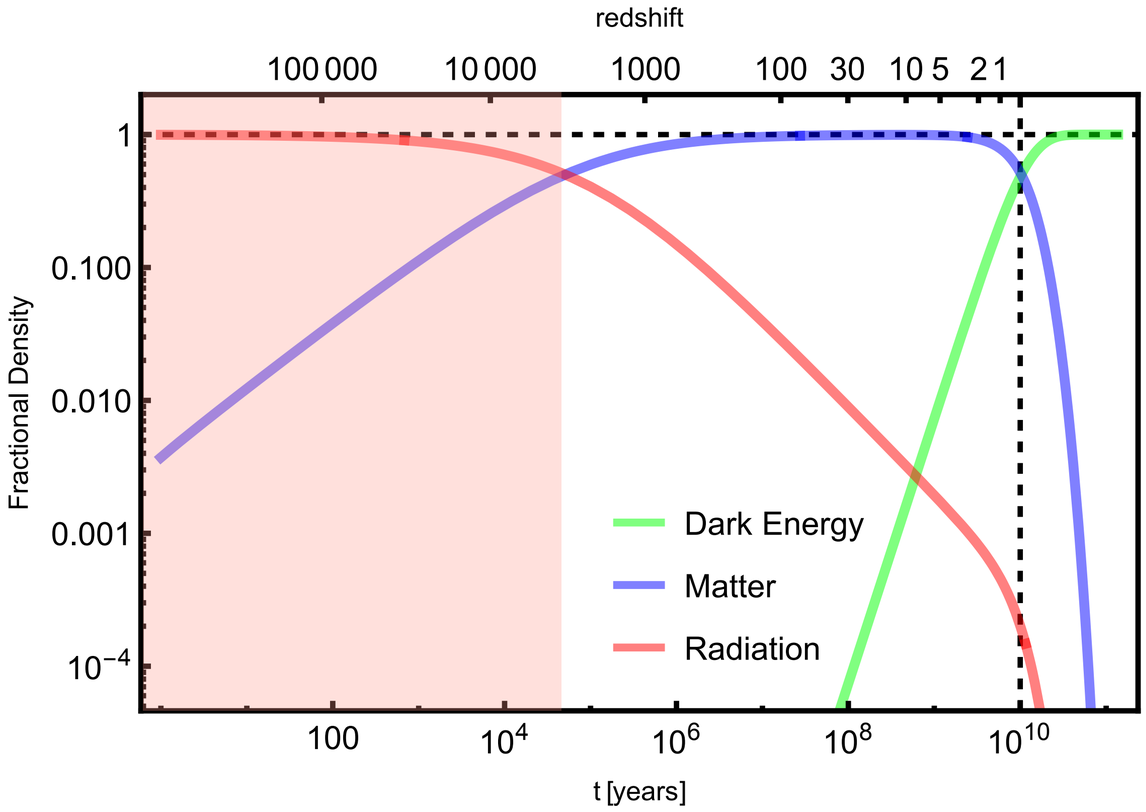

The expanding Universe

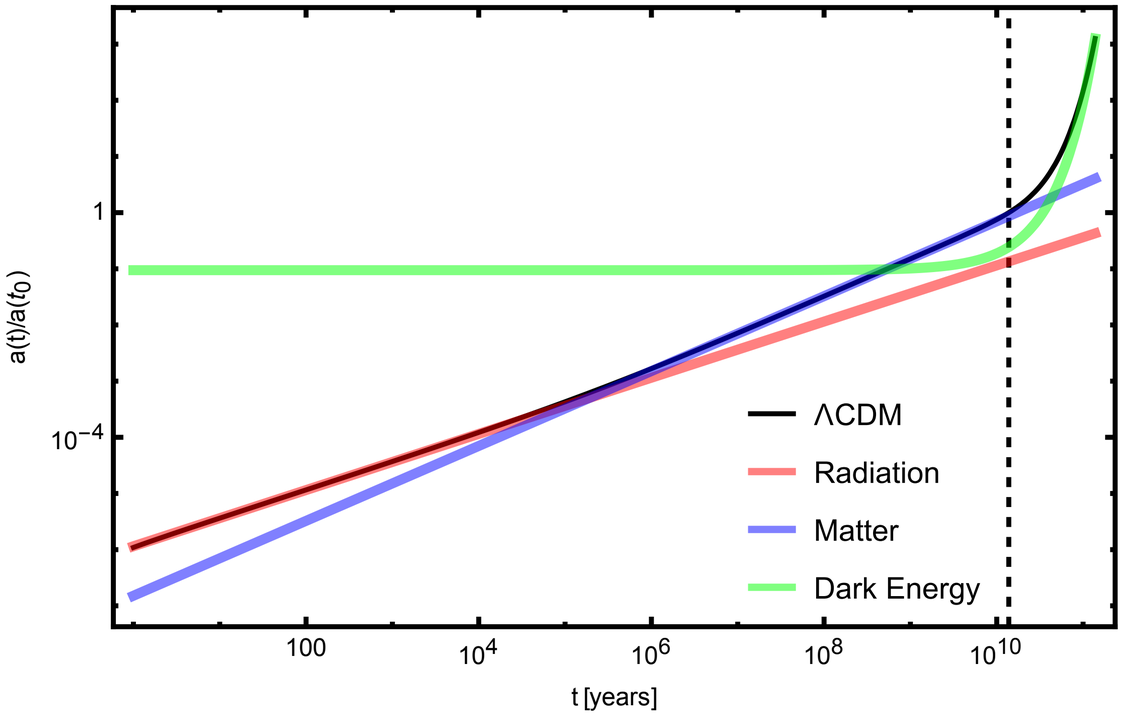

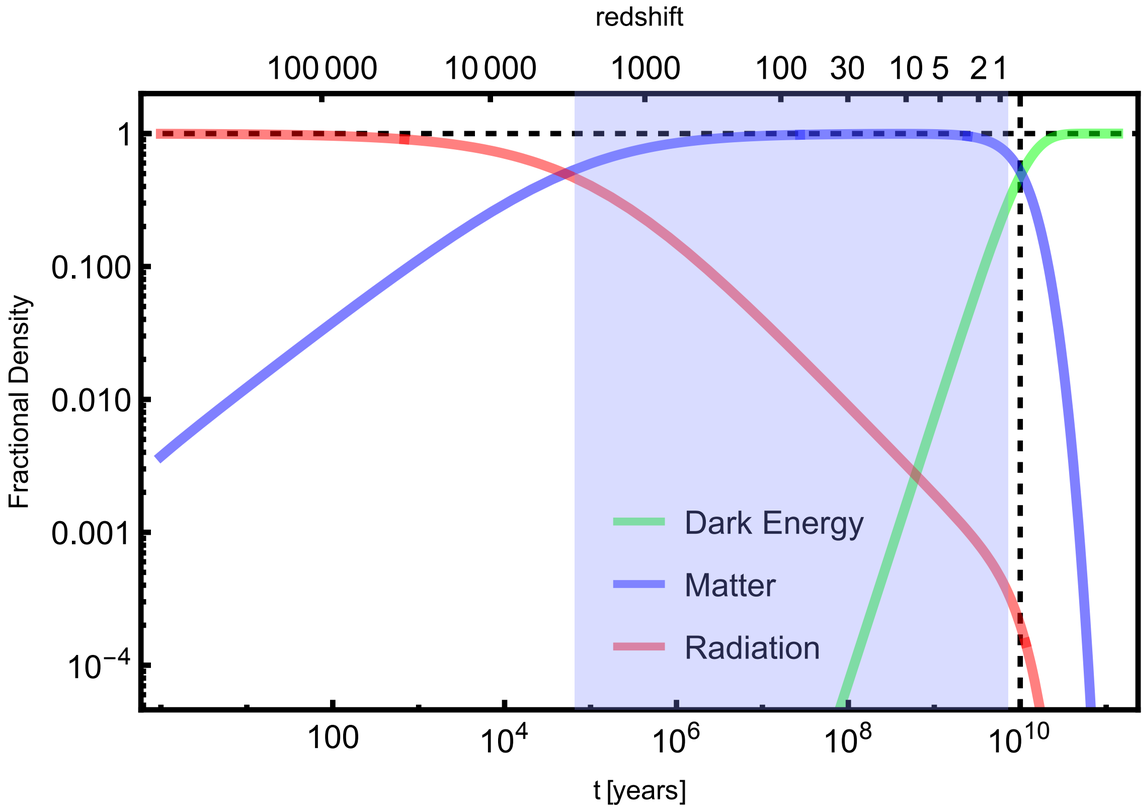

The expanding Universe

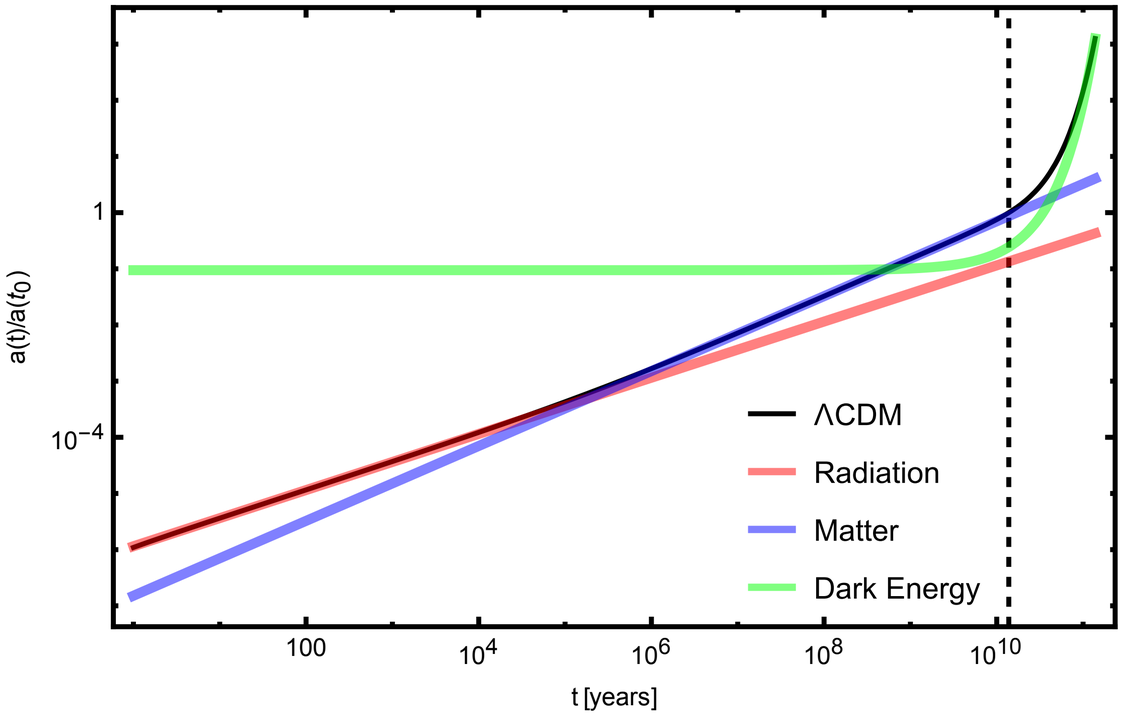

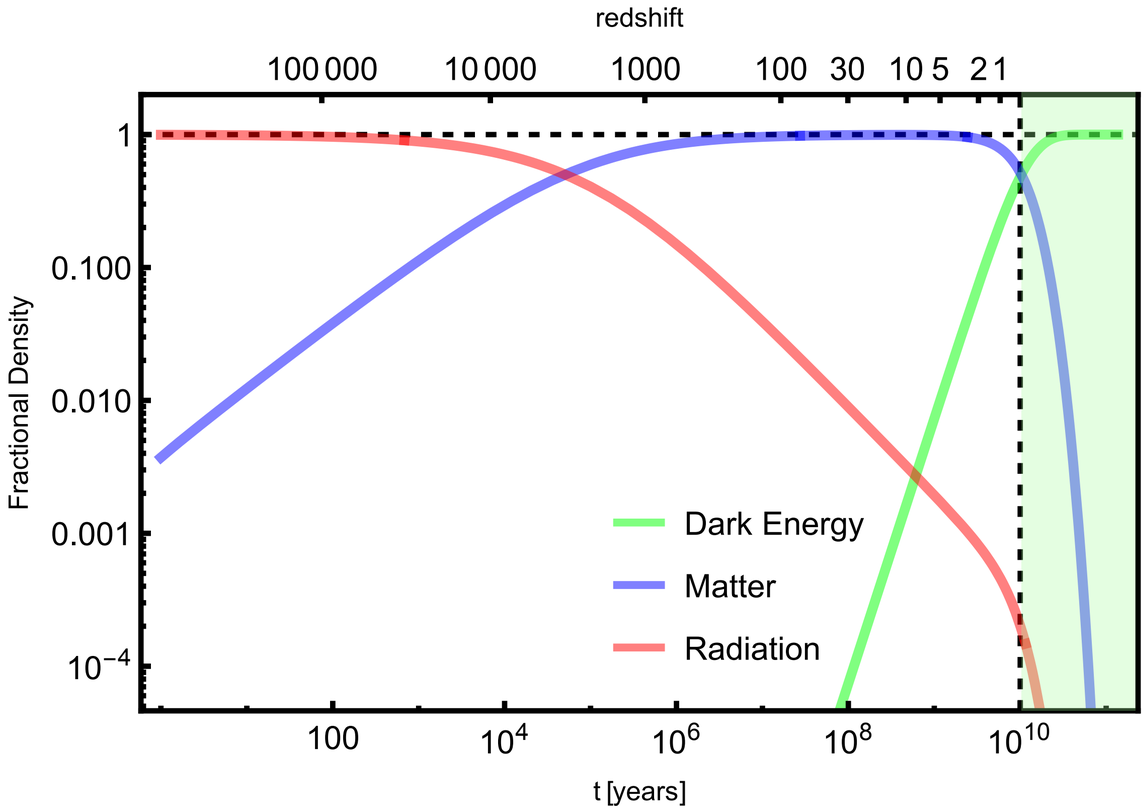

The expanding Universe

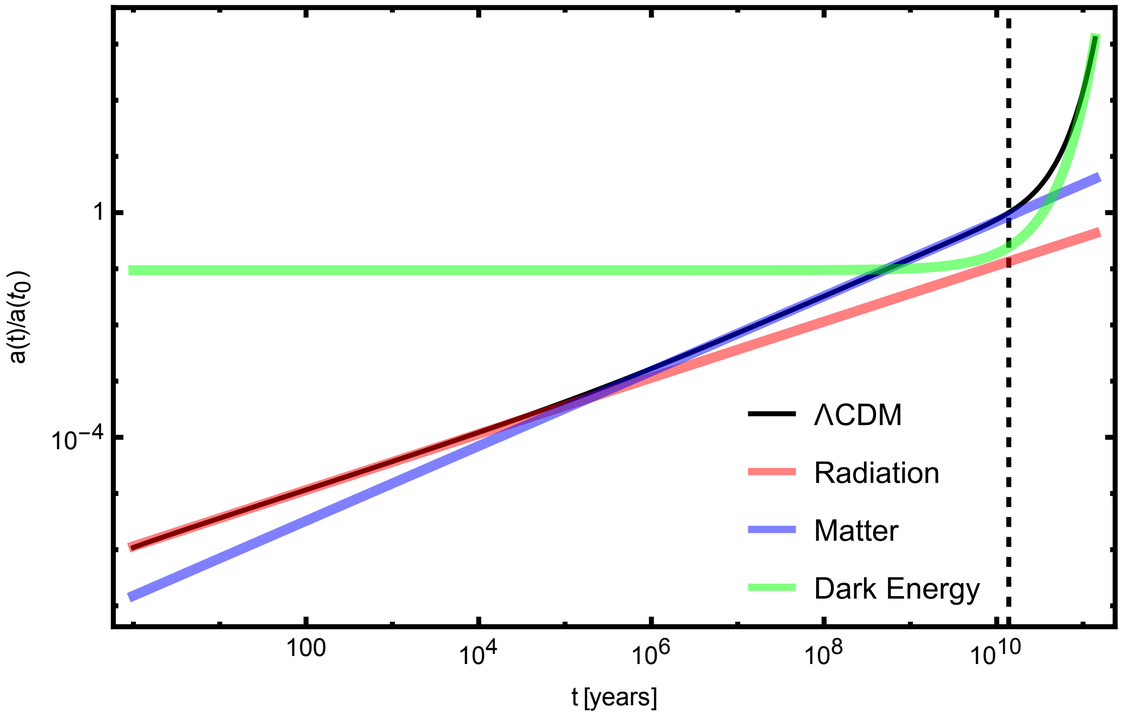

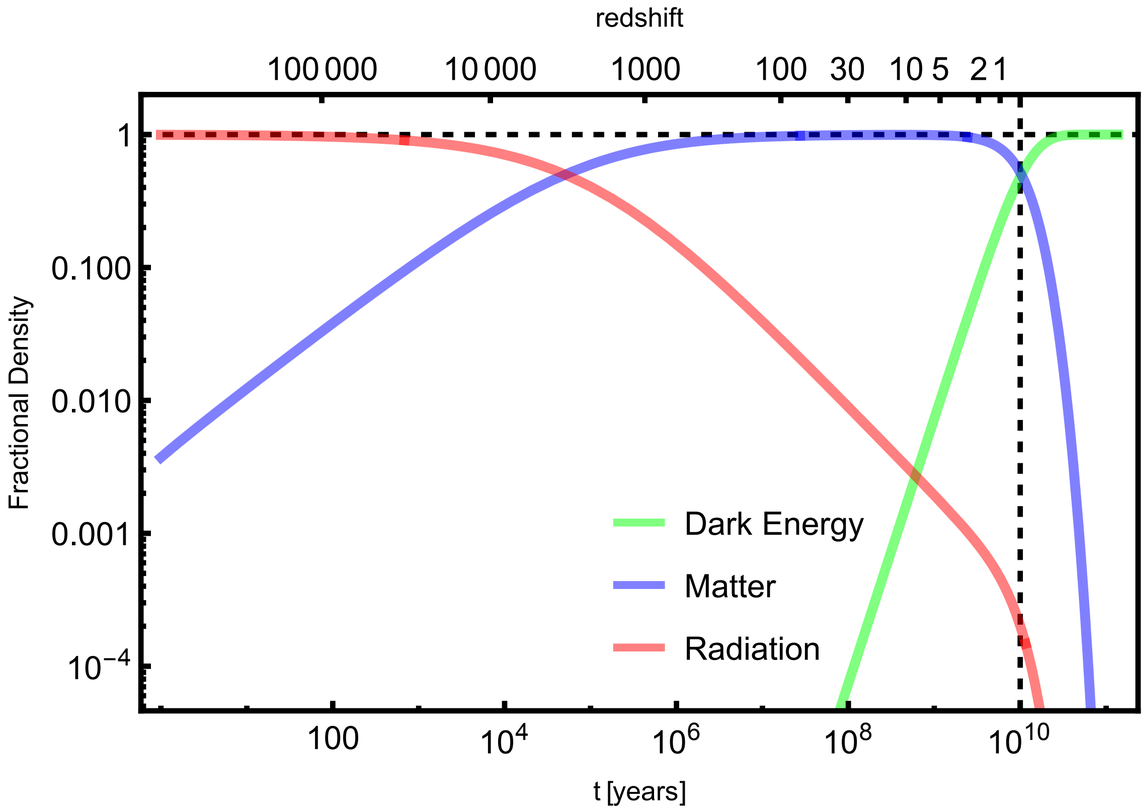

CMB detection

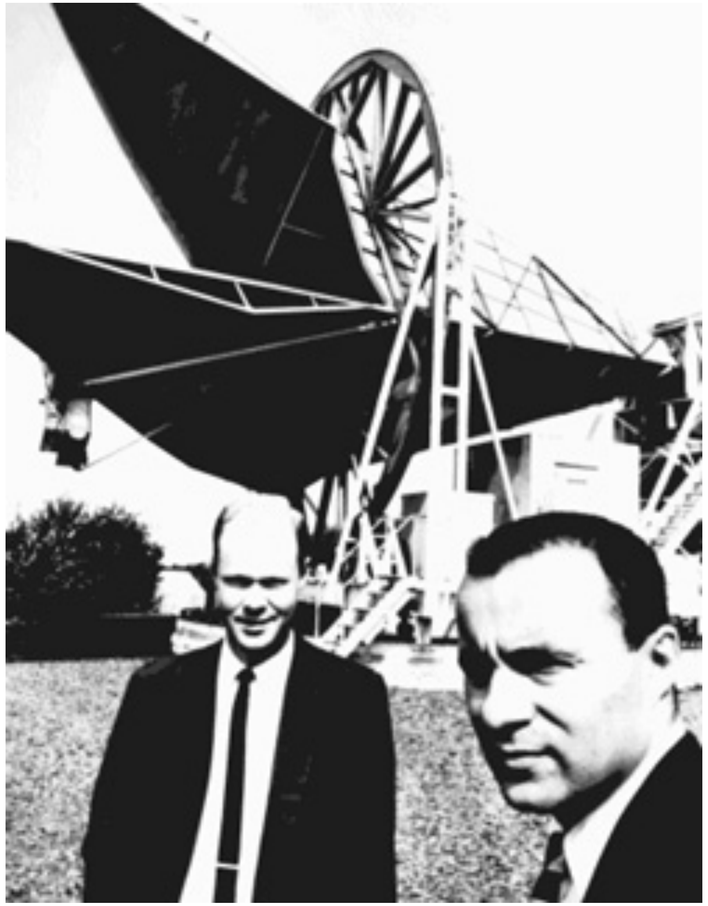

Penzias and Wilson 1964

1978 Nobel prize

1965ApJ.

A MEASUREMENT OF EXCESS ANTENNA TEMPERATURE AT 4080 Mc/s

Measurements of the effective zenith noise temperature of the 20-foot horn-reflector antenna (Crawford, Hogg, and Hunt 1961) at the Crawford Hill Laboratory, Holmdel, New Jersey, at 4080 Mc/s have yielded a value about 3.5° K higher than expected. This excess temperature is, within the limits of our observations, isotropic, unpolarized, and free from seasonal variations (July, 1964–April, 1965). A possible explanation for the observed excess noise temperature is the one given by Dicke, Peebles, Roll, and Wilkinson (1965) in a companion letter in this issue.

The total antenna temperature measured at the zenith is 6.7° K of which 2.3° K is due to atmospheric absorption. The calculated contribution due to ohmic losses in the antenna and back-lobe response is 0.9° K.

The radiometer used in this investigation has been described elsewhere (Penzias and Wilson 1965). It employs a traveling-wave maser, a low-loss (0.027-db) comparison switch, and a liquid helium–cooled reference termination (Penzias 1965). Measurements were made by switching manually between the antenna input and the reference termination. The antenna, reference termination, and radiometer were well matched so that a round-trip return loss of more than 55 db existed throughout the measurement; thus errors in the measurement of the effective temperature due to impedance mismatch can be neglected. The estimated error in the measured value of the total antenna temperature is 0.3° K and comes largely from uncertainty in the absolute calibration of the reference termination.

The contribution to the antenna temperature due to atmospheric absorption was obtained by recording the variation in antenna temperature with elevation angle and employing the secant law. The result, 2.3° ± 0.3° K, is in good agreement with published values (Hogg 1959; DeGrasse, Hogg, Ohm, and Scovil 1959; Ohm 1961).

The contribution to the antenna temperature from ohmic losses is computed to be 0.8° ± 0.4° K. In this calculation we have divided the antenna into three parts: (1) two non-uniform tapers approximately 1 m in total length which transform between the $2\frac{1}{8}$-inch round output waveguide and the 6-inch-square antenna throat opening; (2) a double-choke rotary joint located between these two tapers; (3) the antenna itself. Care was taken to clean and align joints between these parts so that they would not significantly increase the loss in the structure. Appropriate tests were made for leakage and loss in the rotary joint with negative results.

The possibility of losses in the antenna horn due to imperfections in its seams was eliminated by means of a taping test. Taping all the seams in the section near the throat and most of the others with aluminum tape caused no observable change in antenna temperature.

The backlobe response to ground radiation is taken to be less than 0.1° K for two reasons: (1) Measurements of the response of the antenna to a small transmitter located on the ground in its vicinity indicate that the average back-lobe level is more than 30 db below isotropic response. The horn-reflector antenna was pointed to the zenith for these measurements, and complete rotations in azimuth were made with the transmitter in each of ten locations using horizontal and vertical transmitted polarization from each position. (2) Measurements on smaller horn-reflector antennas at these laboratories, using pulsed measuring sets on flat antenna ranges, have consistently shown a back-lobe level of 30 db below isotropic response. Our larger antenna would be expected to have an even lower back-lobe level.

From a combination of the above, we compute the remaining unaccounted-for antenna temperature to be 3.5° ± 1.0° K at 4080 Mc/s. In connection with this result it should be noted that DeGrasse *et al.* (1959) and Ohm (1961) give total system temperatures at 5650 Mc/s and 2390 Mc/s, respectively. From these it is possible to infer upper limits to the background temperatures at these frequencies. These limits are, in both cases, of the same general magnitude as our value.

We are grateful to R. H. Dicke and his associates for fruitful discussions of their results prior to publication. We also wish to acknowledge with thanks the useful comments and advice of A. B. Crawford, D. C. Hogg, and E. A. Ohm in connection with the problems associated with this measurement.

CMB Black Body

2.728 ± 0.004 K

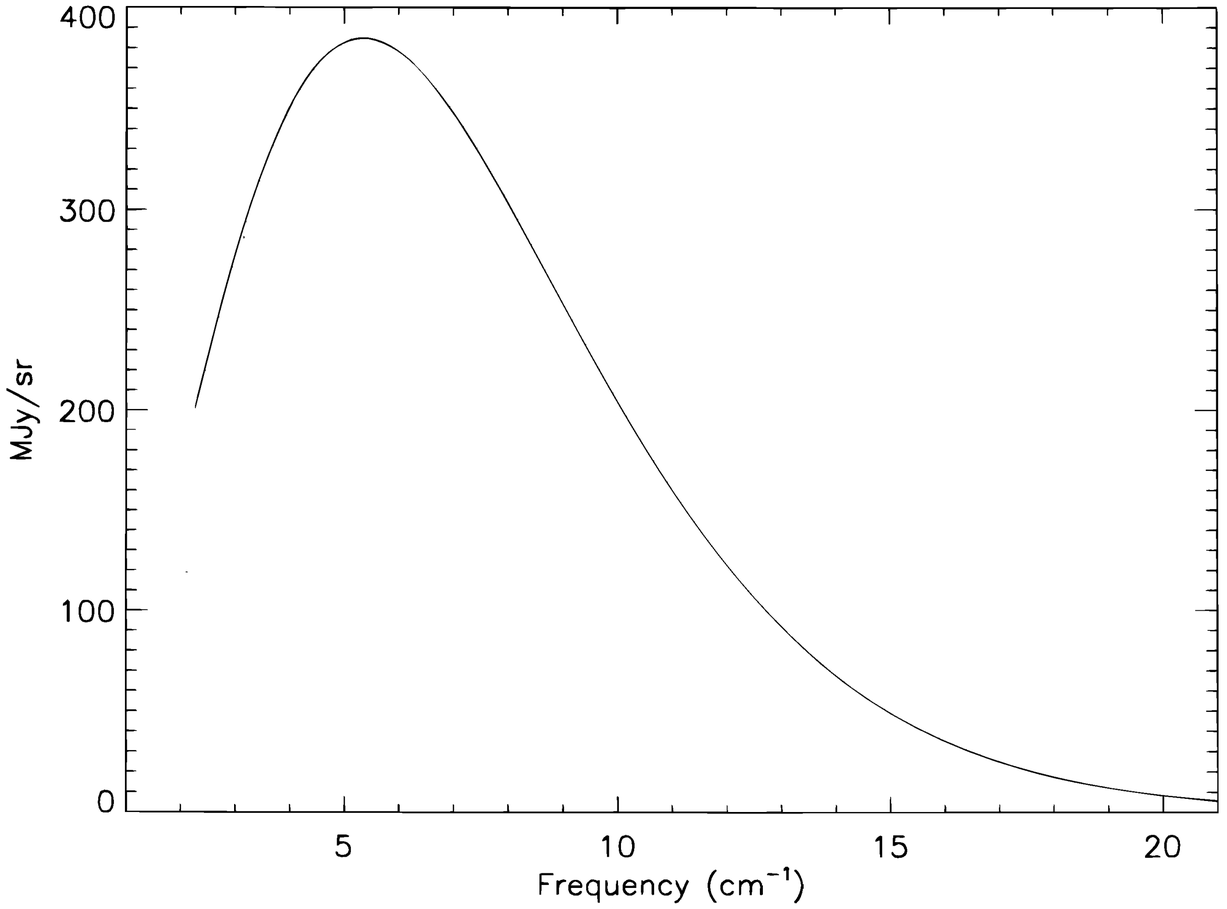

COBE FIRAS 1996

FIG. 4.—Uniform spectrum and fit to Planck blackbody (T). Uncertainties are a small fraction of the line thickness.

Thermal history

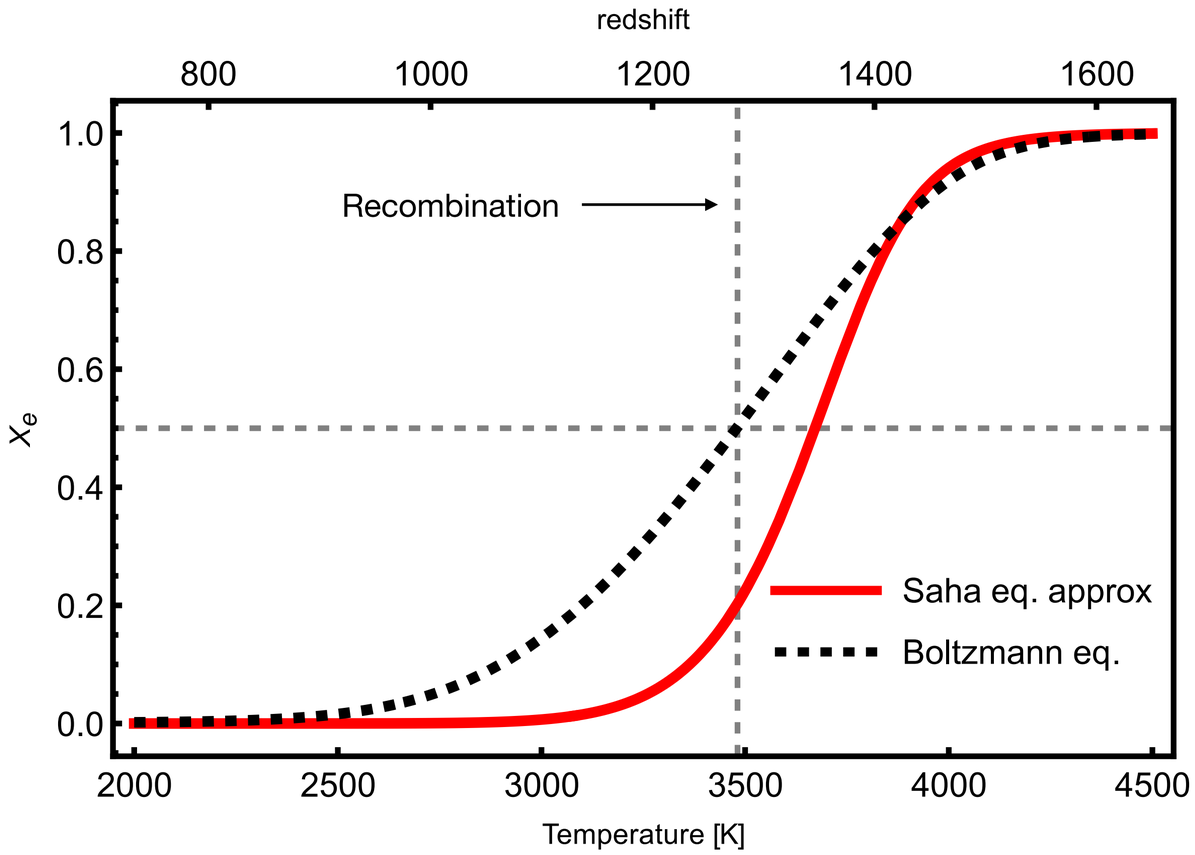

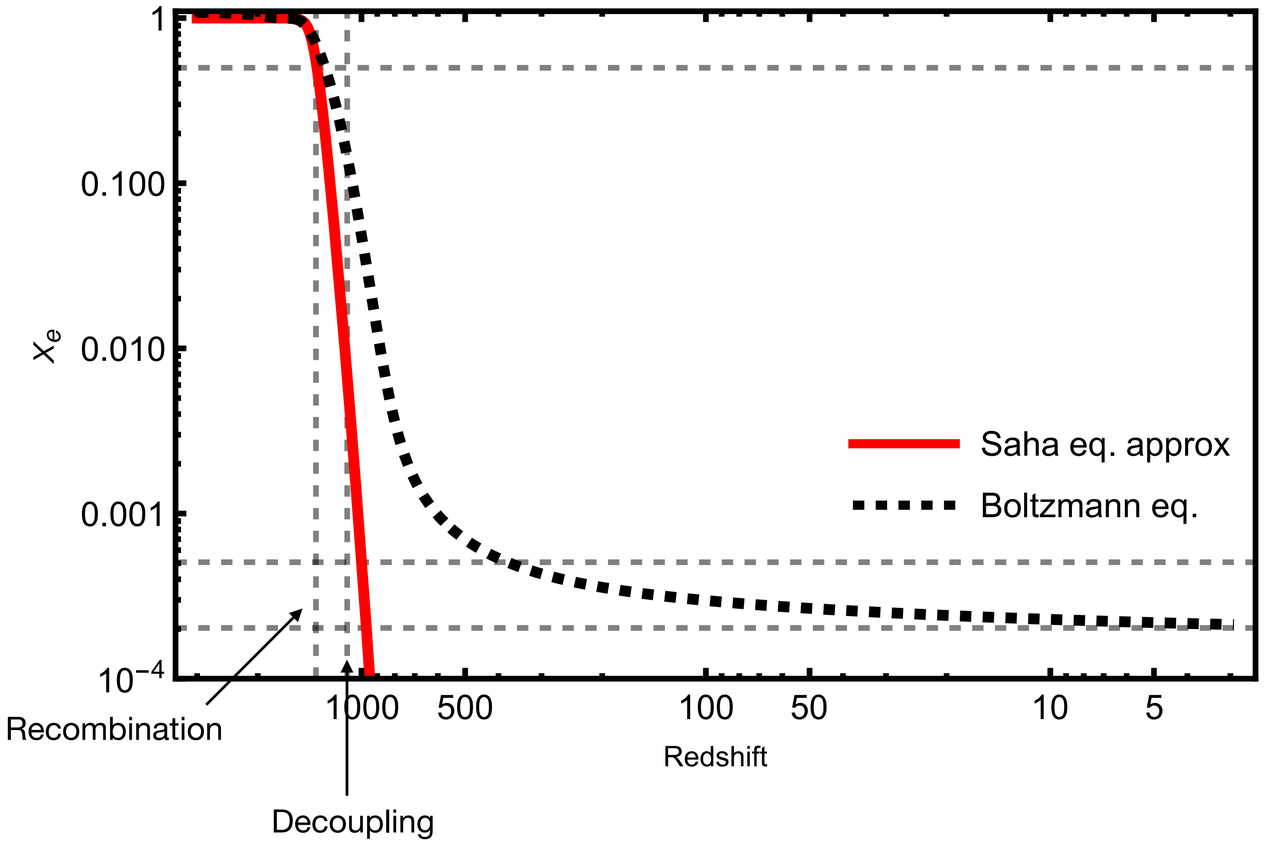

CMB anisotropies

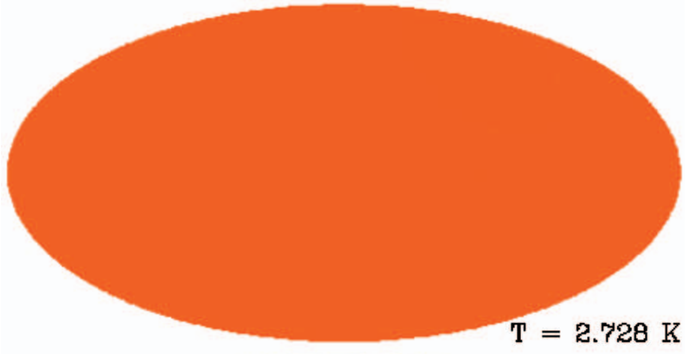

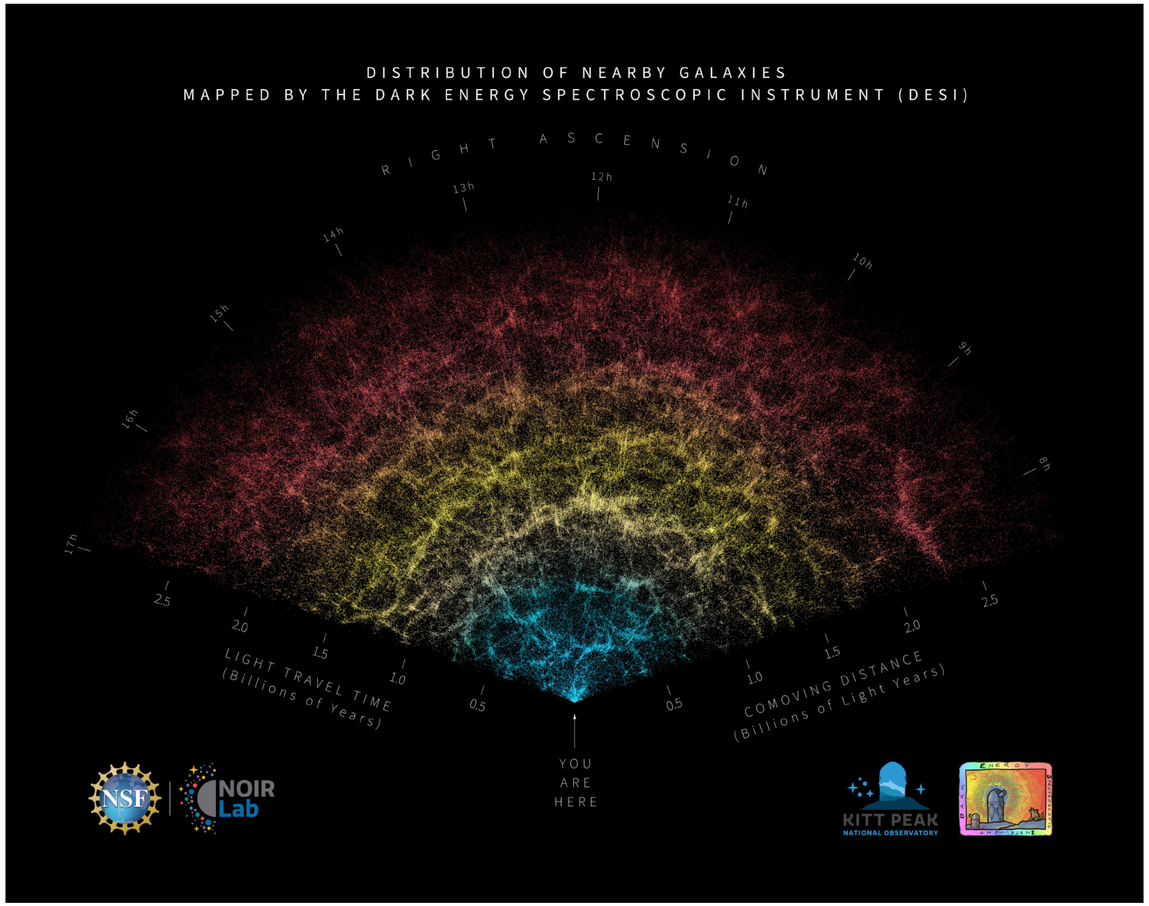

$$n_{\mathrm{CMB}} = \frac{16\pi\zeta(3)}{c^3}\left(\frac{k_B T_{\mathrm{CMB}}}{h}\right)^3 \simeq 410\ \mathrm{cm}^{-3}$$

$$n_\gamma \sim 1\ \mathrm{cm}^{-3}$$

CMB anisotropies

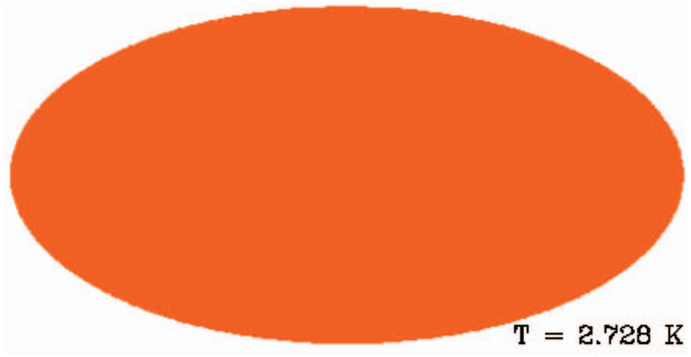

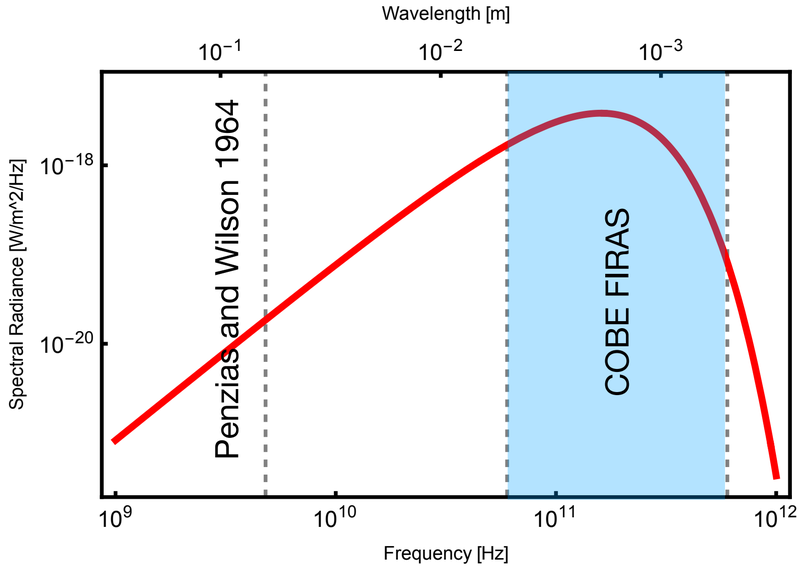

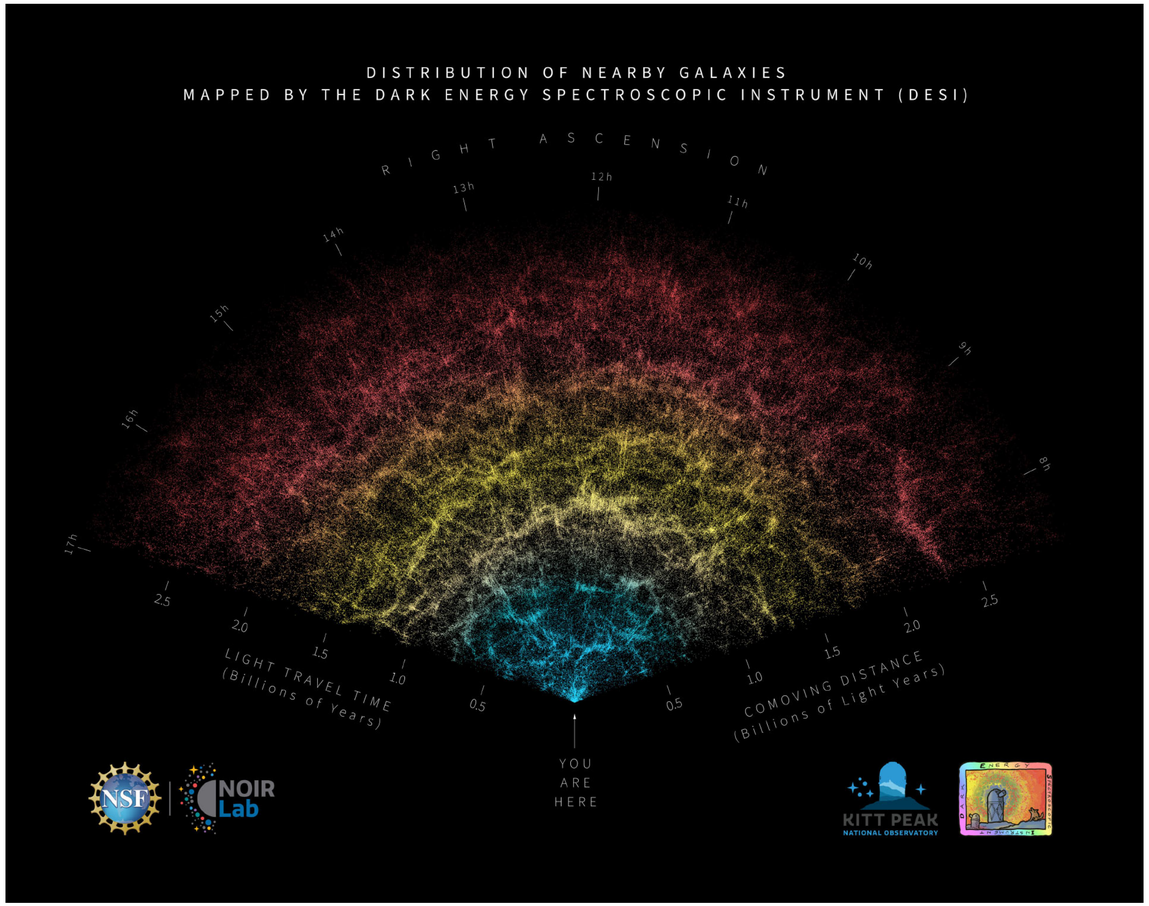

$$n_{\mathrm{CMB}} = \frac{16\pi\zeta(3)}{c^3}\left(\frac{k_B T_{\mathrm{CMB}}}{h}\right)^3 \simeq 410\ \mathrm{cm}^{-3}$$

$$n_\gamma \sim 1\ \mathrm{cm}^{-3}$$

CMB anisotropies

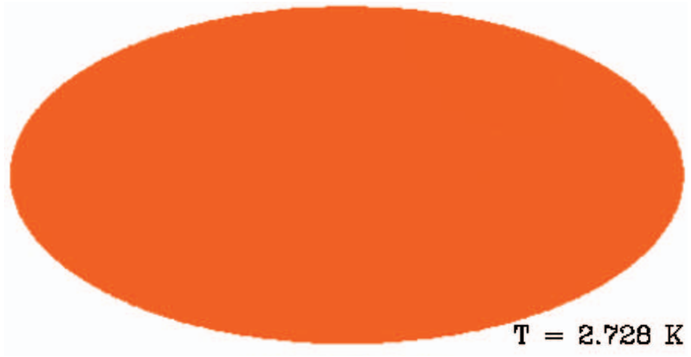

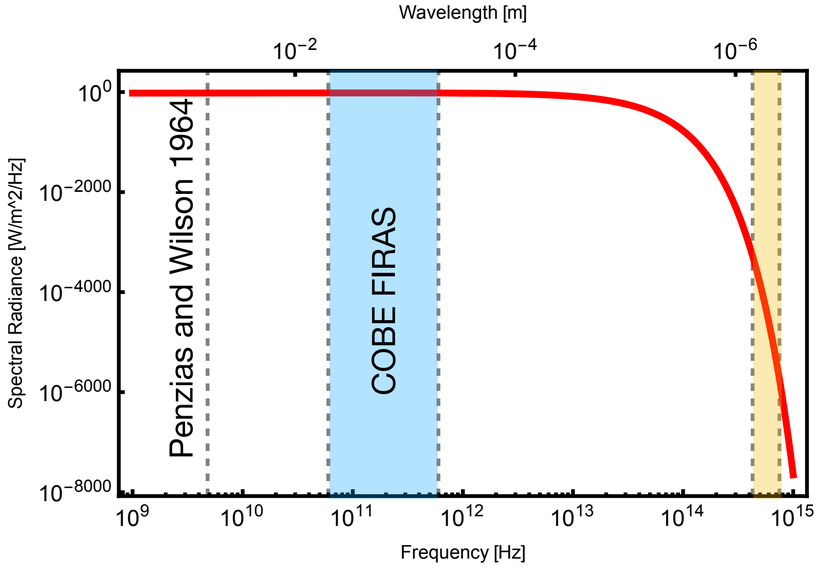

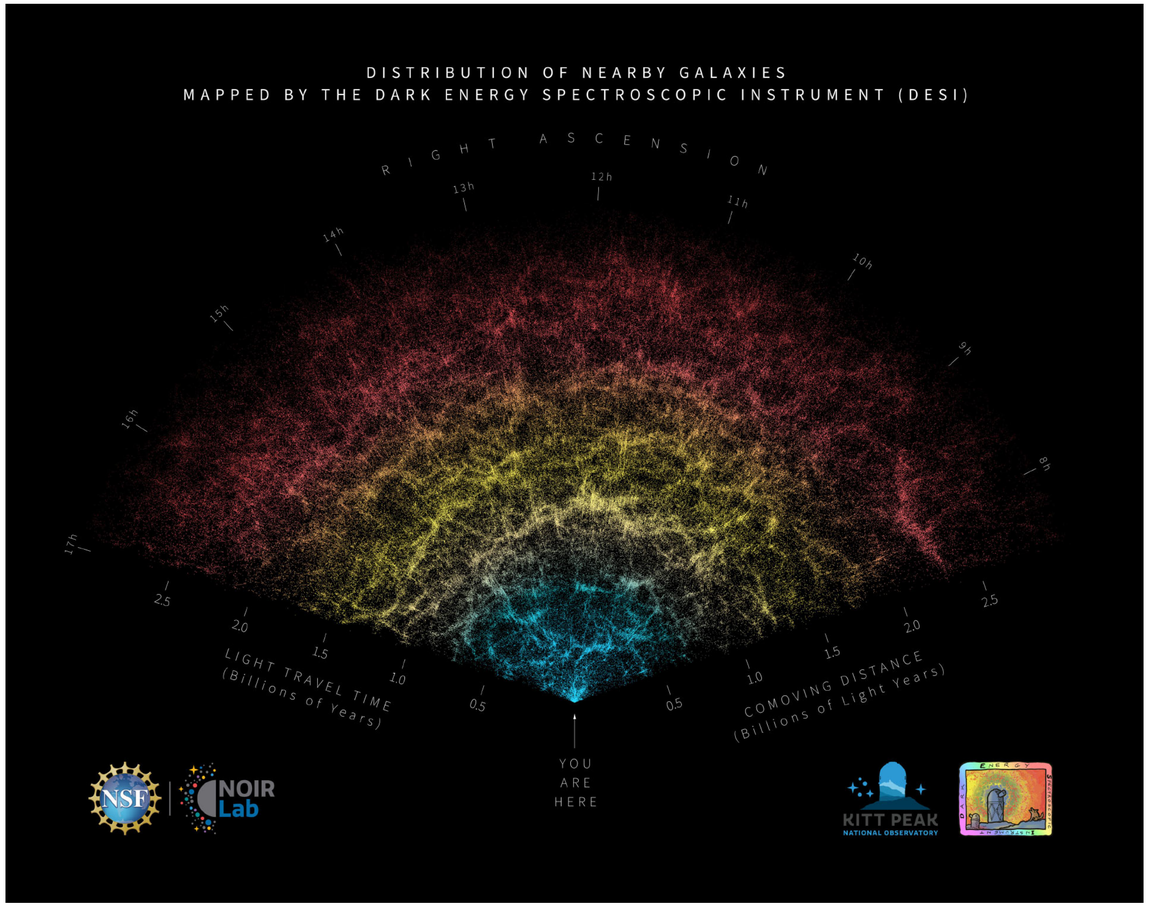

$$n_{\mathrm{CMB}} = \frac{16\pi\zeta(3)}{c^3}\left(\frac{k_B T_{\mathrm{CMB}}}{h}\right)^3 \simeq 410\ \mathrm{cm}^{-3}$$

$$n_\gamma \sim 1\ \mathrm{cm}^{-3}$$

CMB anisotropies

Dipole

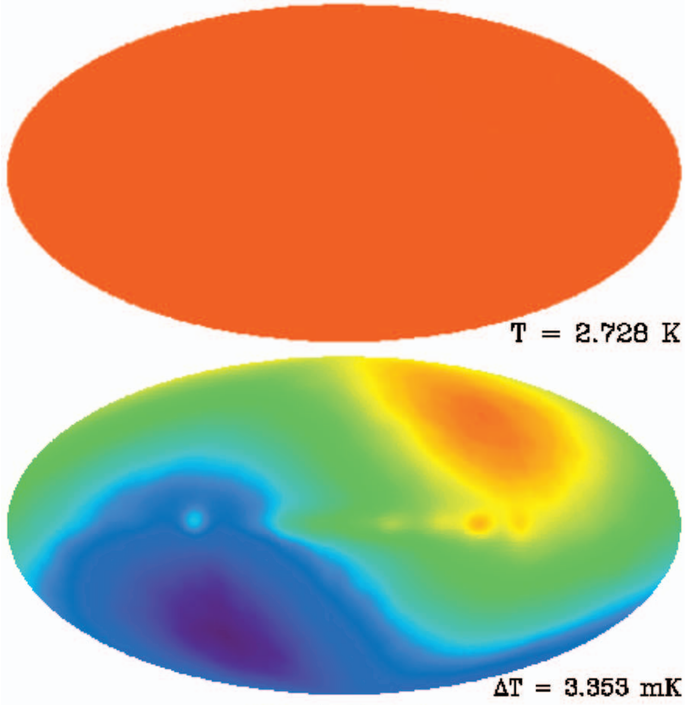

$\times 10^3$

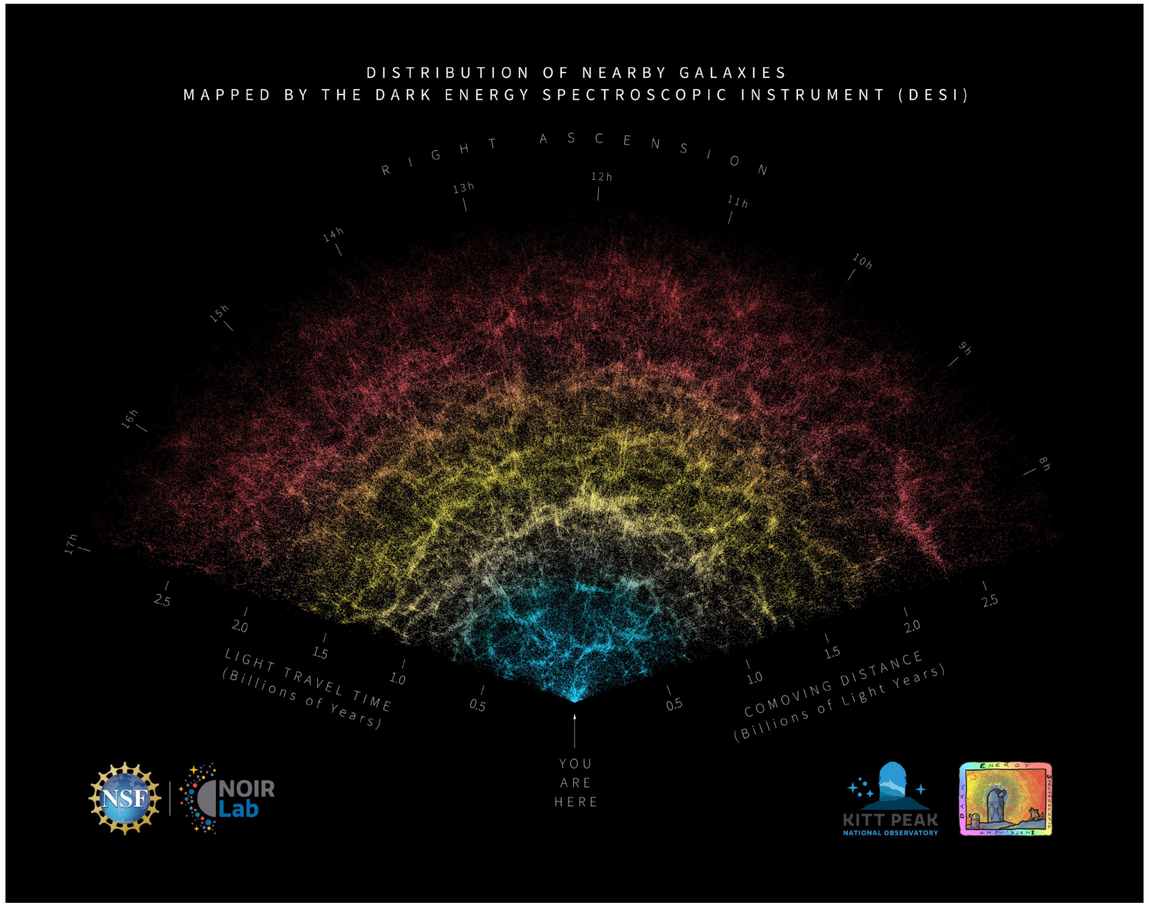

CMB anisotropies

Dipole

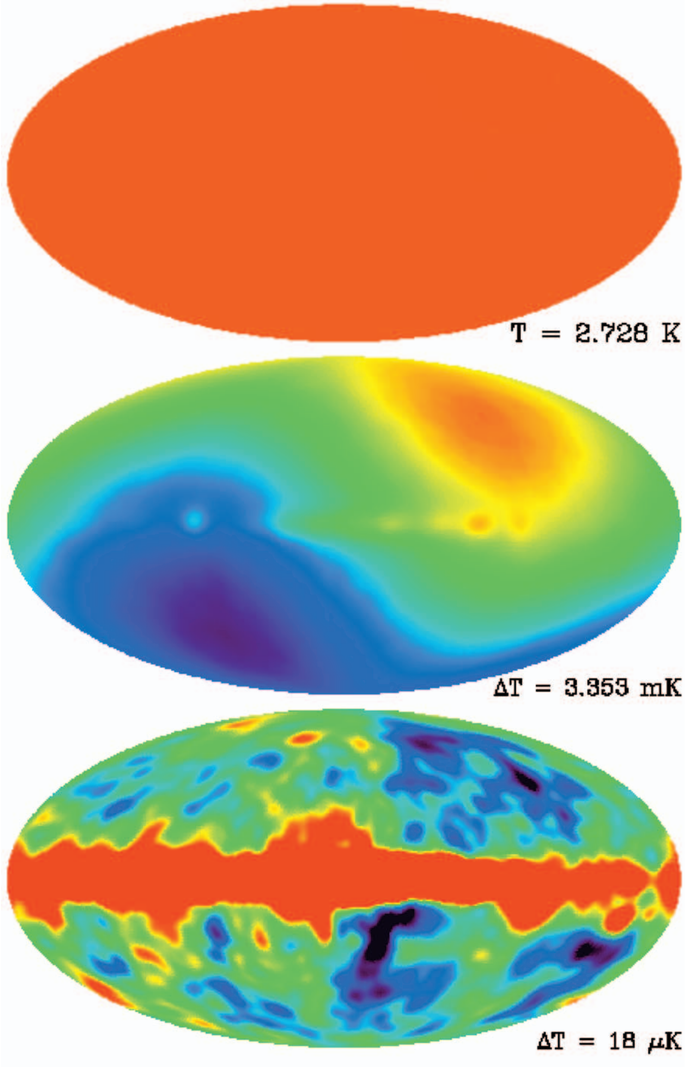

$\times 10^3$

$\times 10^5$

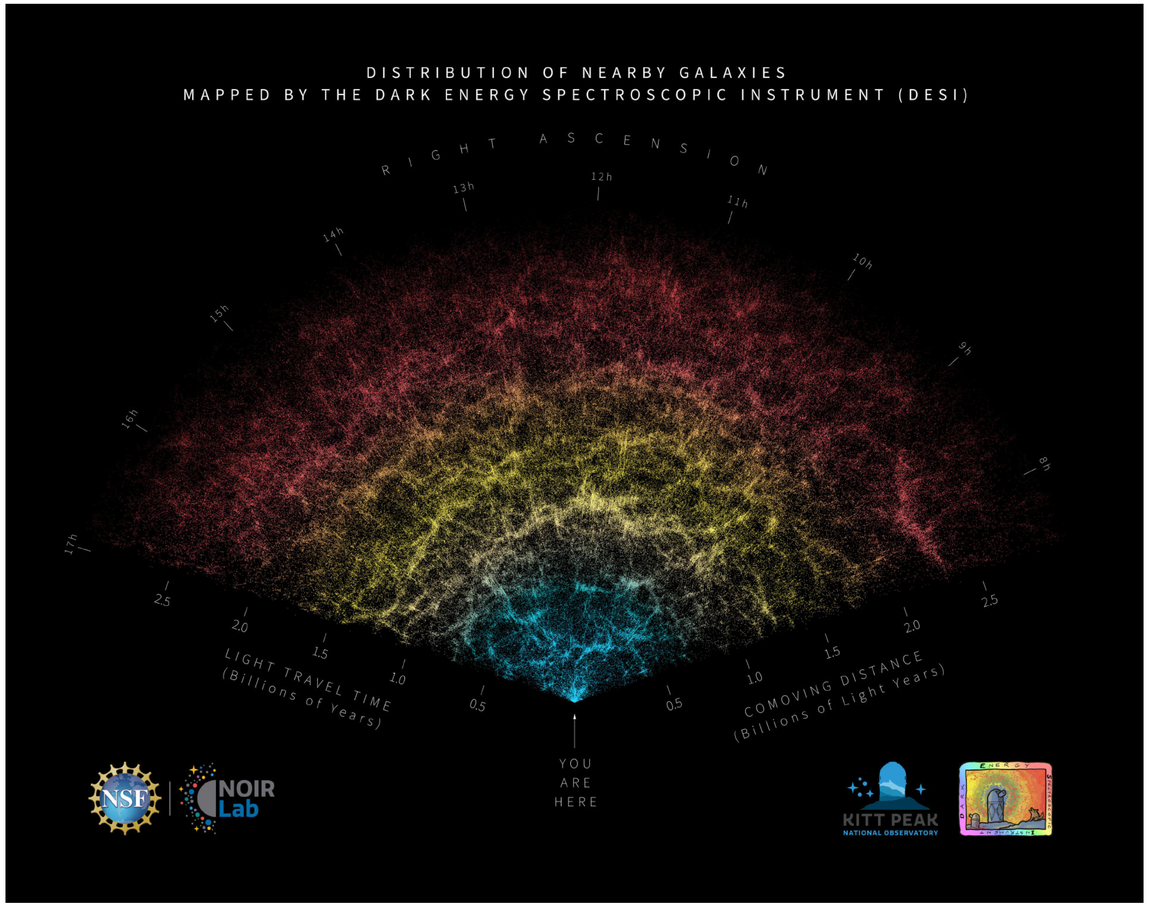

CMB anisotropies

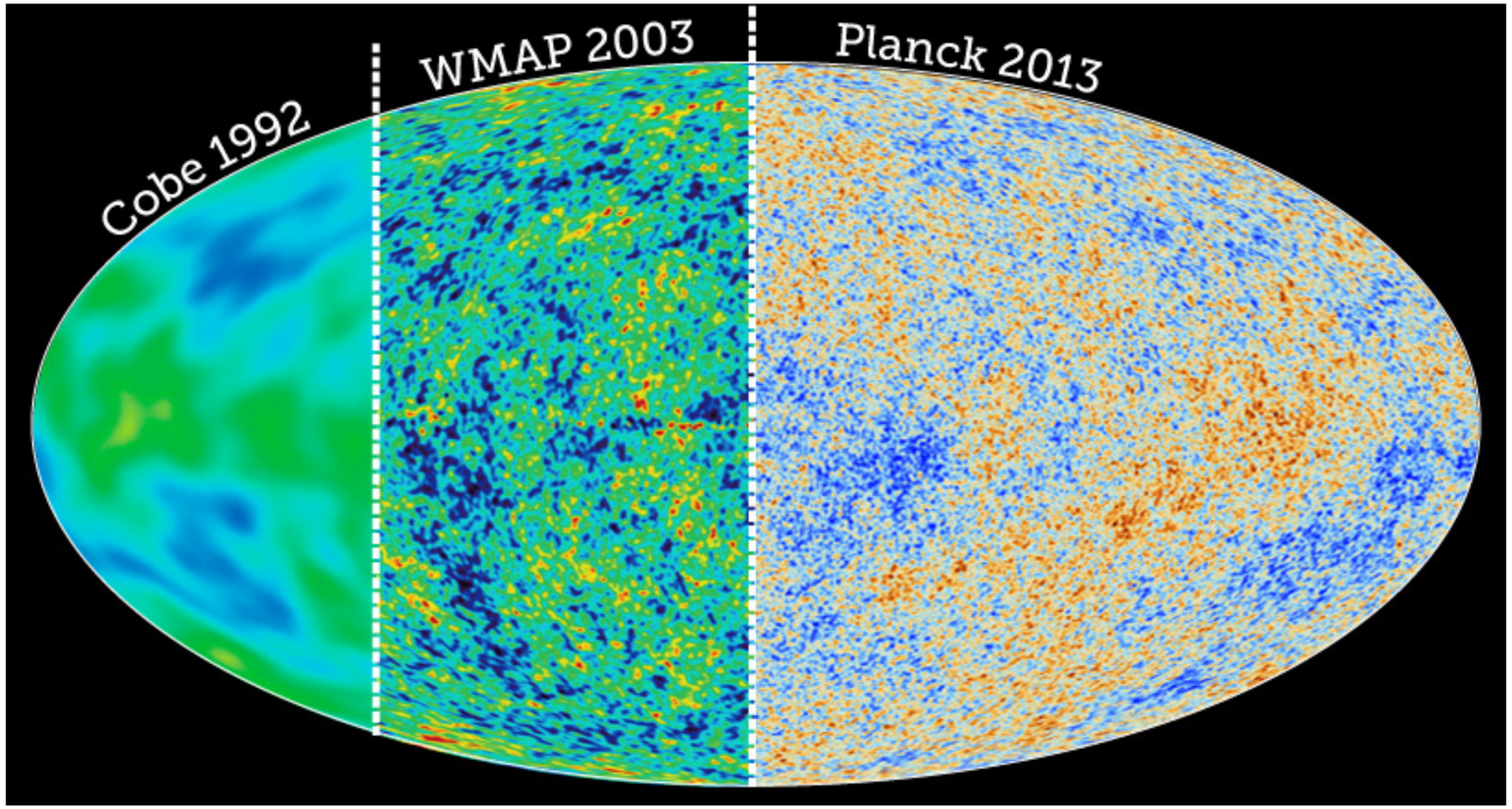

CMB anisotropies

$$C_\ell = 2\pi \int d\mu \xi(\mu) \mathscr{L}_\ell(\mu)$$

$$\cos\theta = \mu = \mathbf{n}\cdot\mathbf{n}'$$

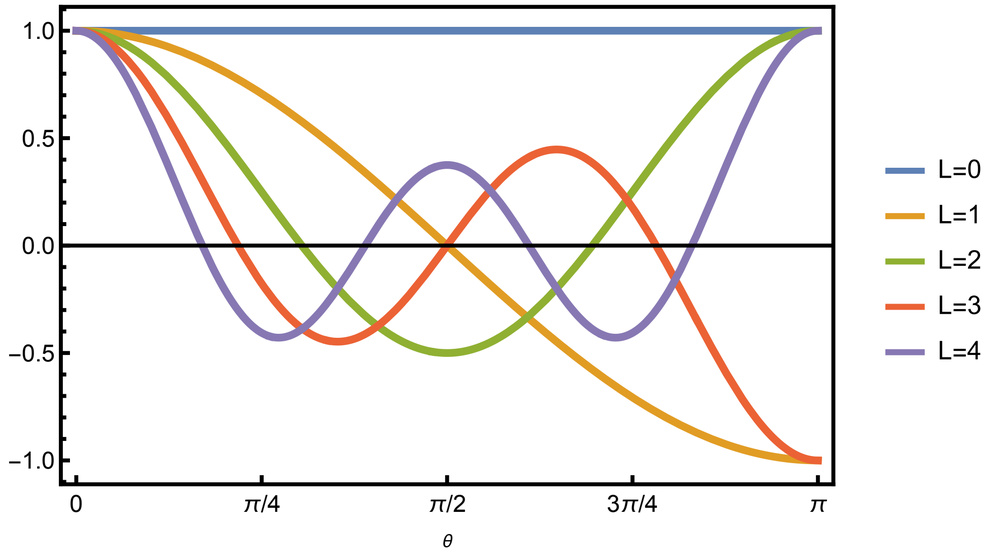

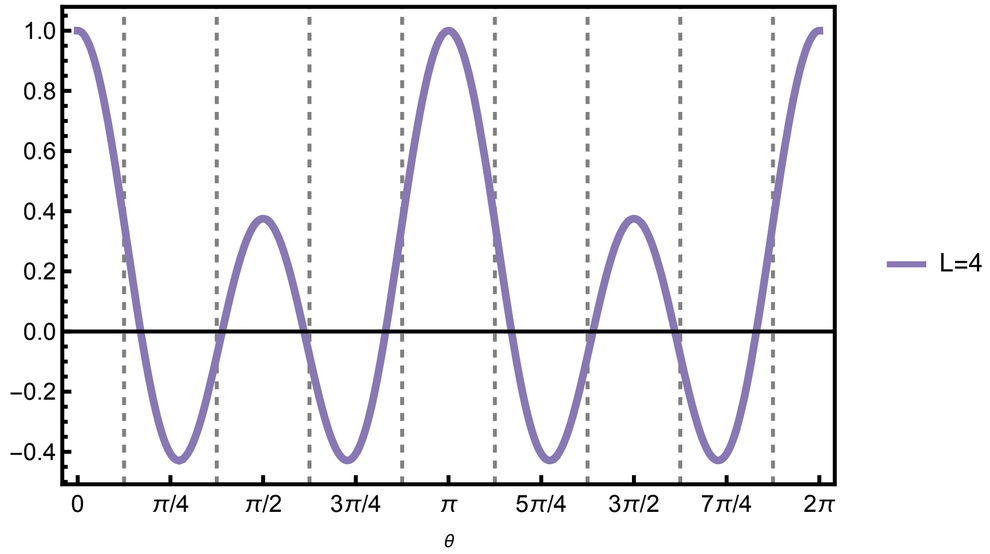

$$\theta \sim \lambda \sim \pi/\ell = 180^o/\ell$$

CMB anisotropies

$$C_\ell = 2\pi \int d\mu \xi(\mu) \mathscr{L}_\ell(\mu) = 2\pi \int_0^\pi d\theta \sin\theta \xi(\theta) \mathscr{L}_\ell(\cos\theta)$$

$$\cos\theta = \mu = \mathbf{n} \cdot \mathbf{n}'$$

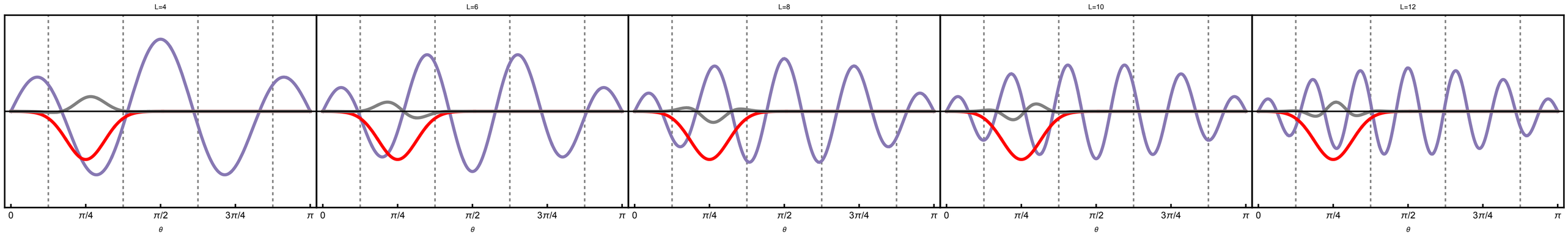

$$\xi(\theta) = -\frac{1}{4} \exp\left(-\frac{(\theta - \frac{\pi}{4})^2}{2(0.2)^2} \right)$$

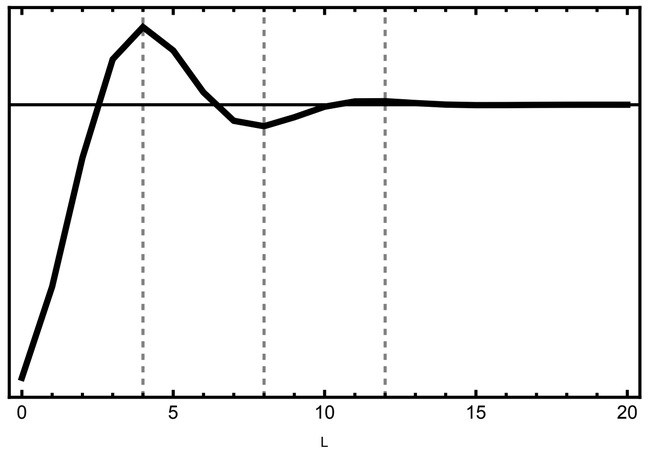

CMB anisotropies

$$C_\ell = 2\pi \int d\mu \xi(\mu) \mathscr{L}_\ell(\mu) = 2\pi \int_0^\pi d\theta \sin\theta \xi(\theta) \mathscr{L}_\ell(\cos\theta)$$

$$\cos\theta = \mu = \mathbf{n} \cdot \mathbf{n}'$$

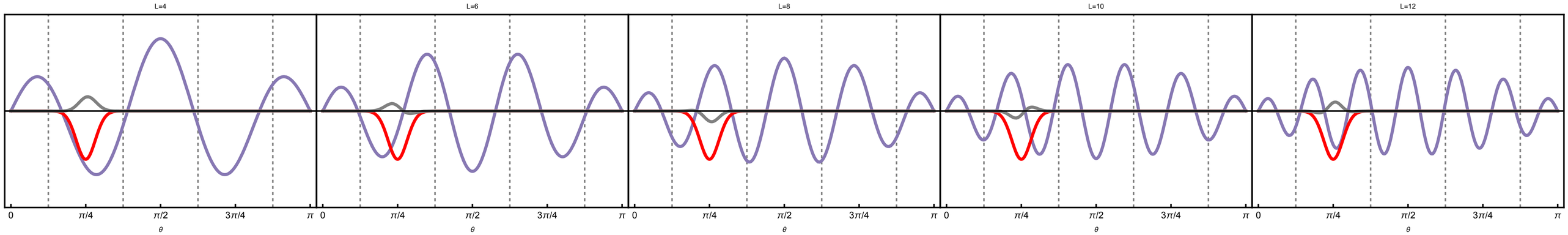

$$\xi(\theta) = -\frac{1}{4} \exp\left(-\frac{(\theta - \frac{\pi}{4})^2}{2(0.1)^2} \right)$$

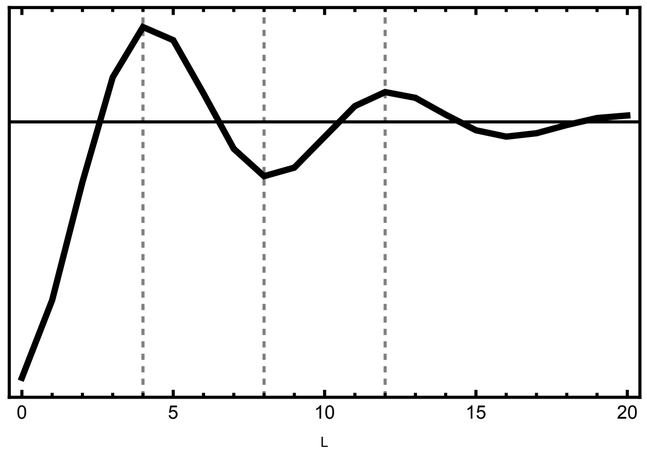

CMB anisotropies

1-degree scale imprinted in CMB map

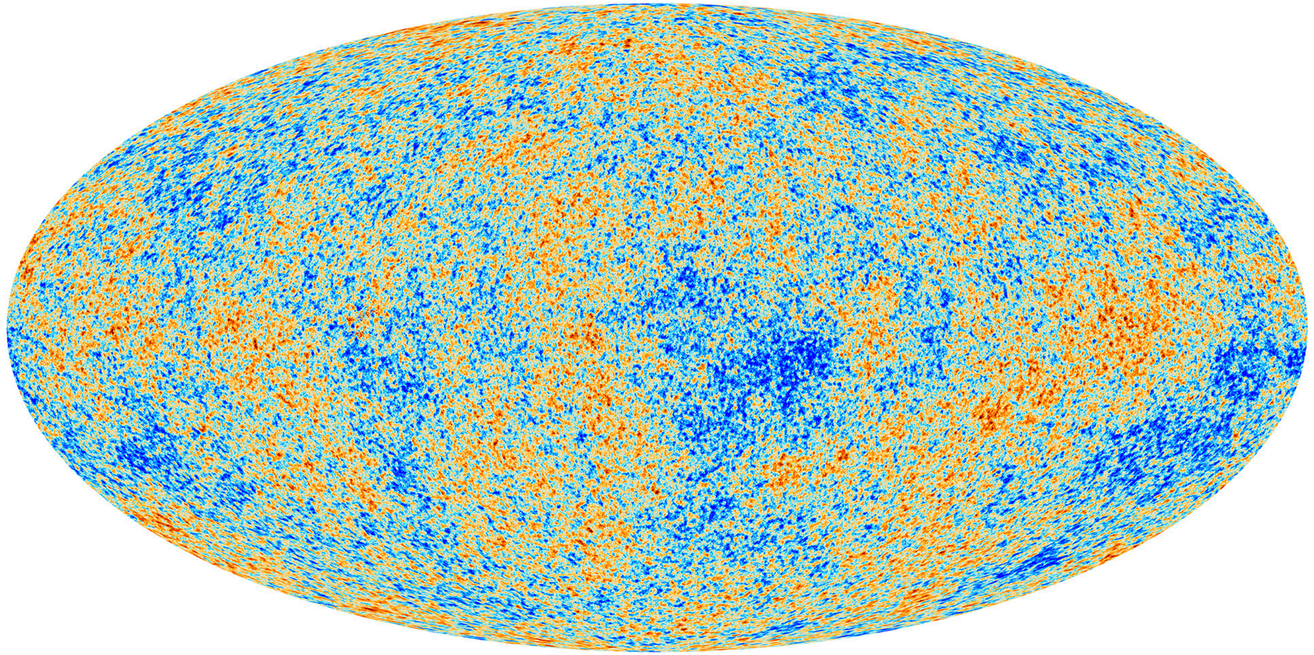

$$\theta \sim \lambda \sim \pi/\ell = 180^o/\ell$$

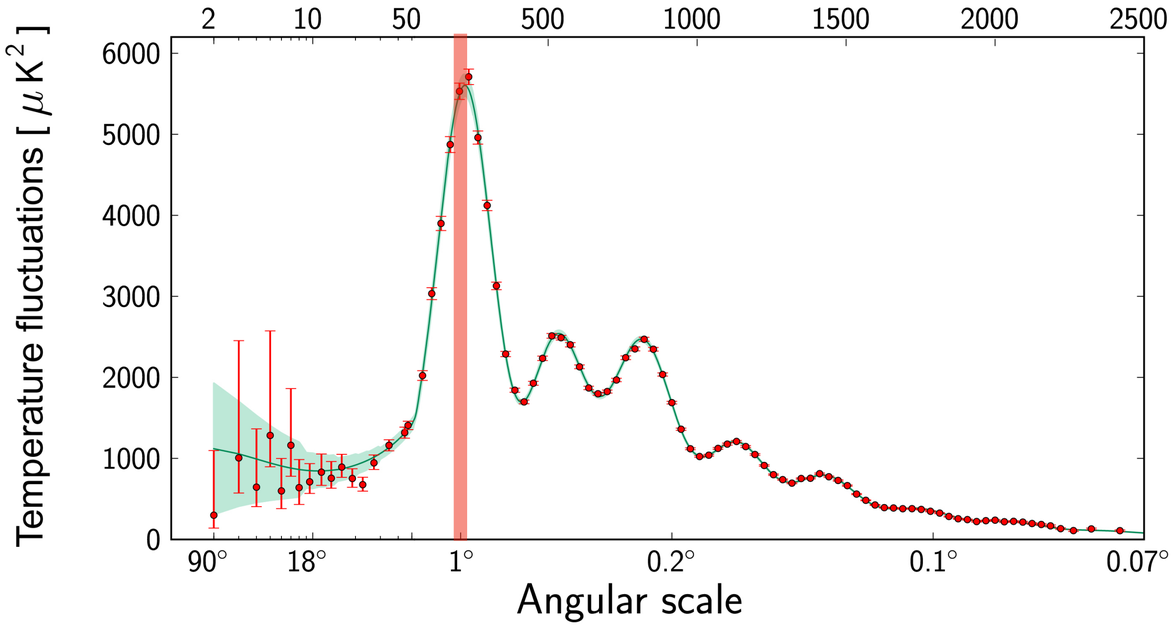

https://chrisnorth.github.io/planckapps/Simulator/#

Spherical Bessel Functions

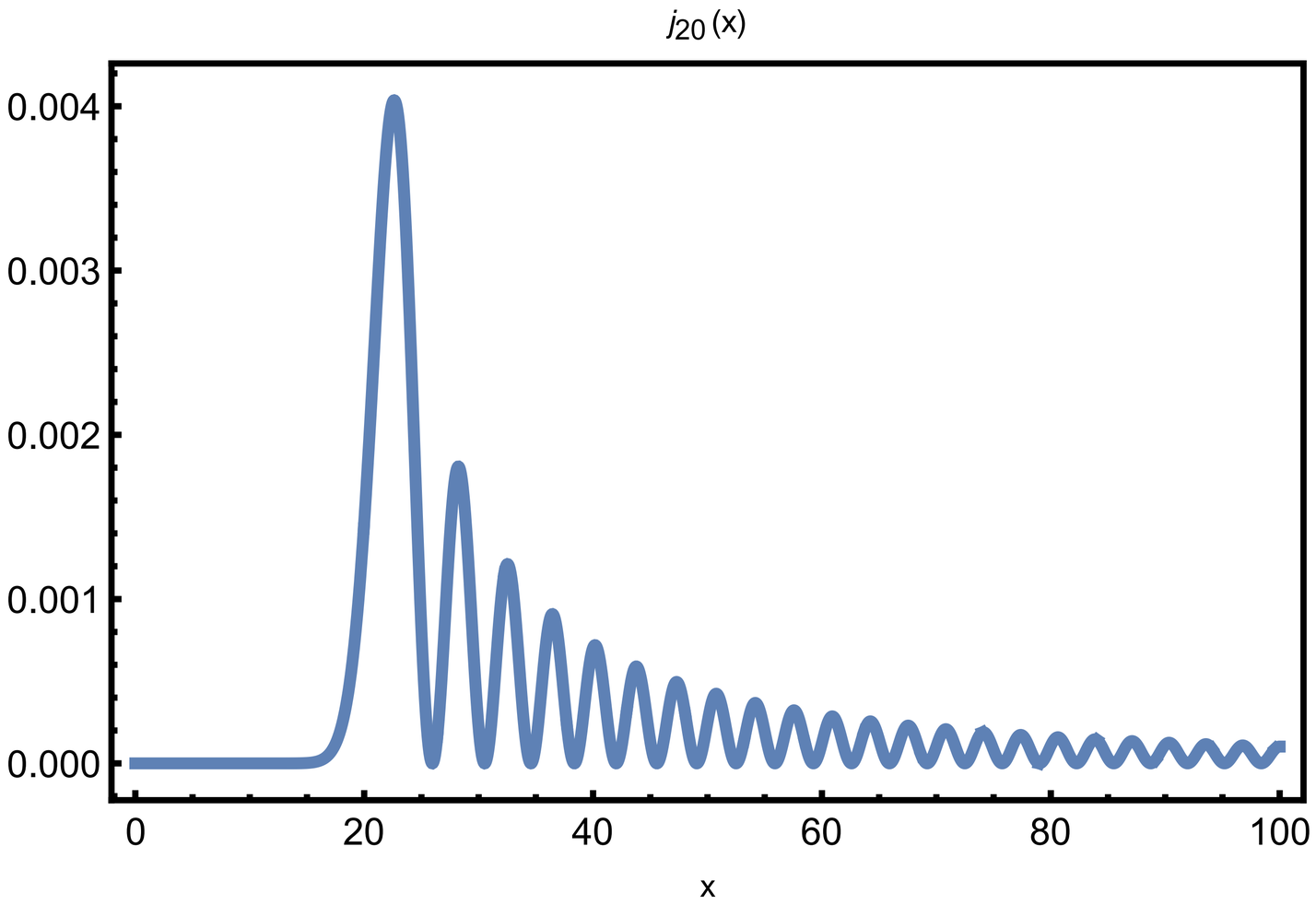

CMB anisotropies

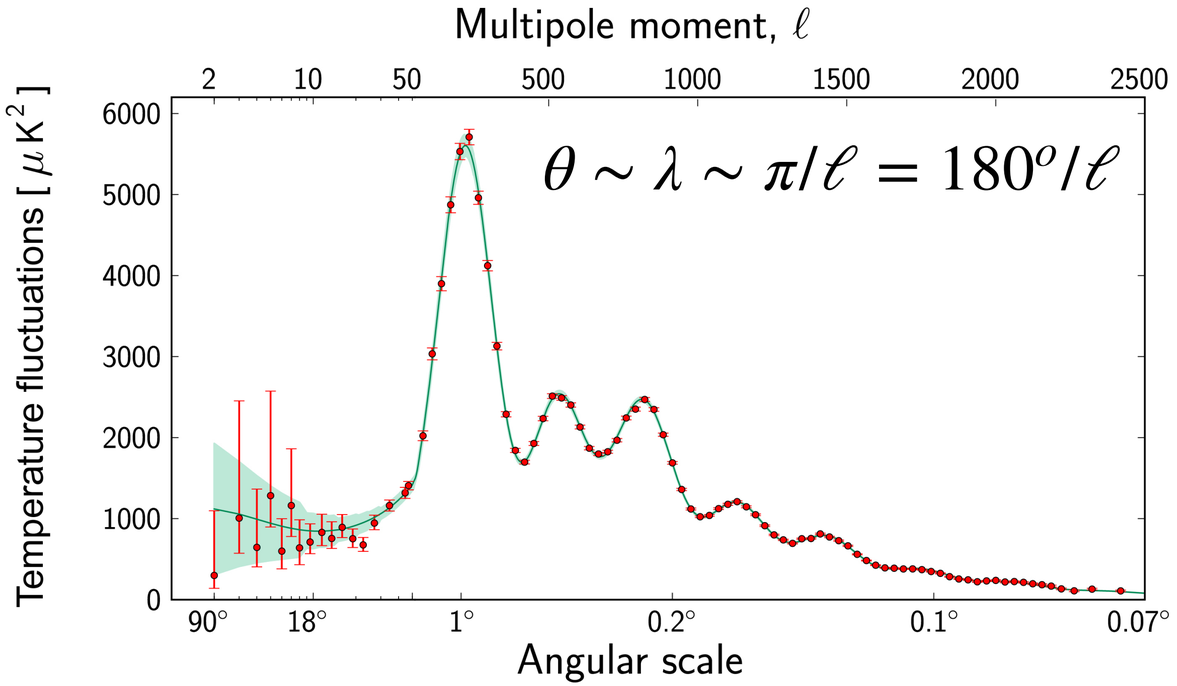

$$\frac{\ell\left(\ell+1\right)}{2\pi}C_\ell^S \sim \frac{A_s}{25}\cos^2\left(\frac{\ell}{\chi_s}r_*\right)$$

- ☑ flat spectrum at $\ell \ll \chi_*/r_*$
- ☐ peaks at $\dfrac{\ell}{\chi_*}r_* = n\pi$
- ☐ oscillation not around 0
- ☐ different peaks amplitude
- ☐ absence of first trough at $\ell = \pi/2\ \chi_*/r_*$
- ☐ suppression of power on small scales

CMB anisotropies

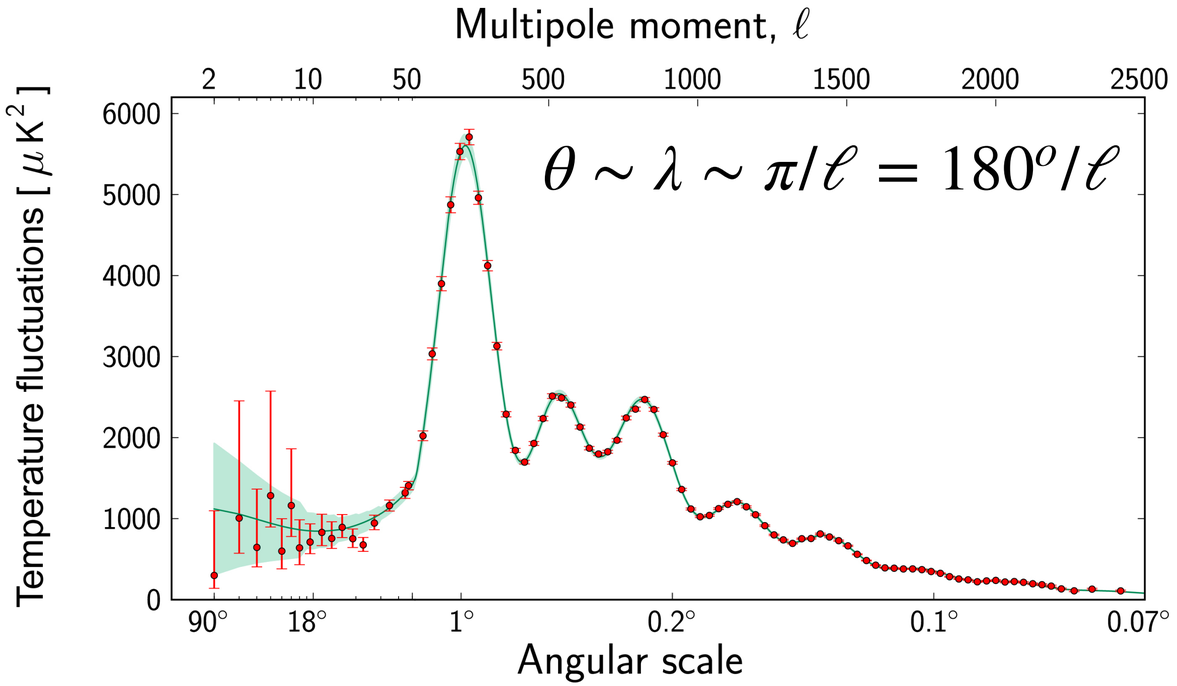

$$\frac{\ell\left(\ell+1\right)}{2\pi}C_\ell^S \sim \frac{A_s}{25}\cos^2\left(\frac{\ell}{\chi_s}r_*\right)$$

First peak position

$$\ell_1 = \pi\frac{\chi_*}{r_*} \sim 290$$

with $r_* \sim 100$ Mpc/h
and $\chi_* \sim 9340$ Mpc/h

CMB anisotropies

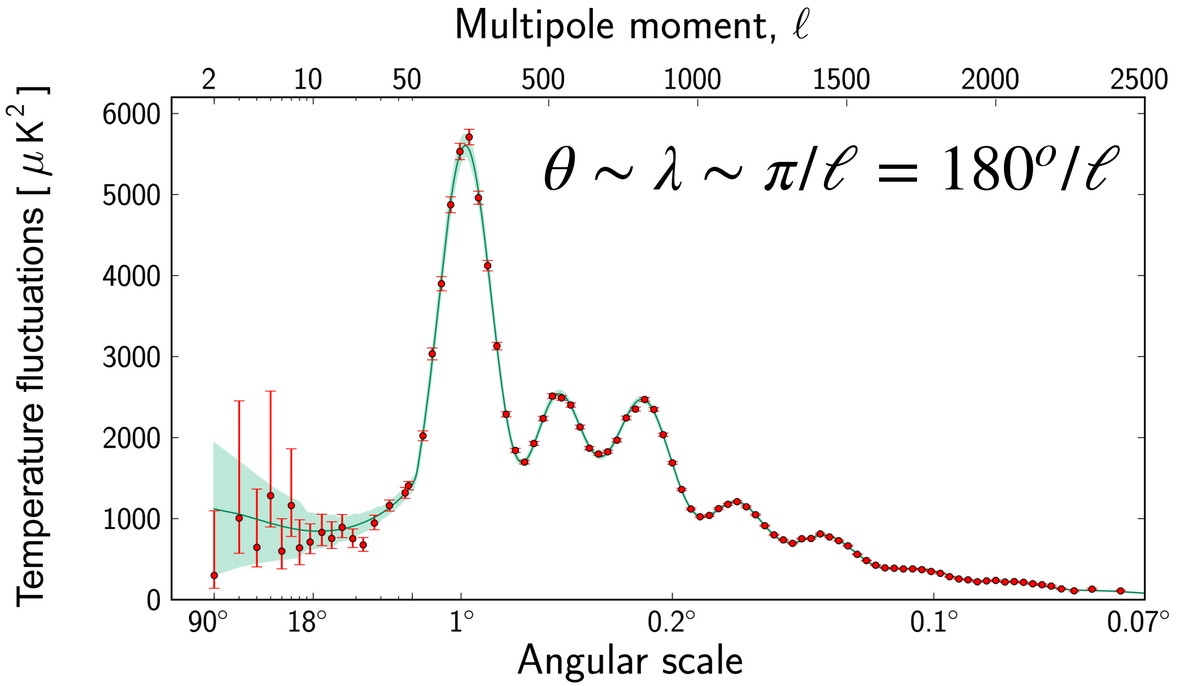

$$\frac{\ell\left(\ell+1\right)}{2\pi}C_\ell^S \sim \frac{A_s}{25}\cos^2\left(\frac{\ell}{\chi_s}r_*\right)$$

- ☑ flat spectrum at $\ell \ll \chi_*/r_*$
- ☑ peaks at $\dfrac{\ell}{\chi_*}r_* = n\pi$
- ☐ oscillation not around 0
- ☐ different peaks amplitude
- ☐ absence of first trough at $\ell = \pi/2\ \chi_*/r_*$
- ☐ suppression of power on small scales

Acoustic Oscillations

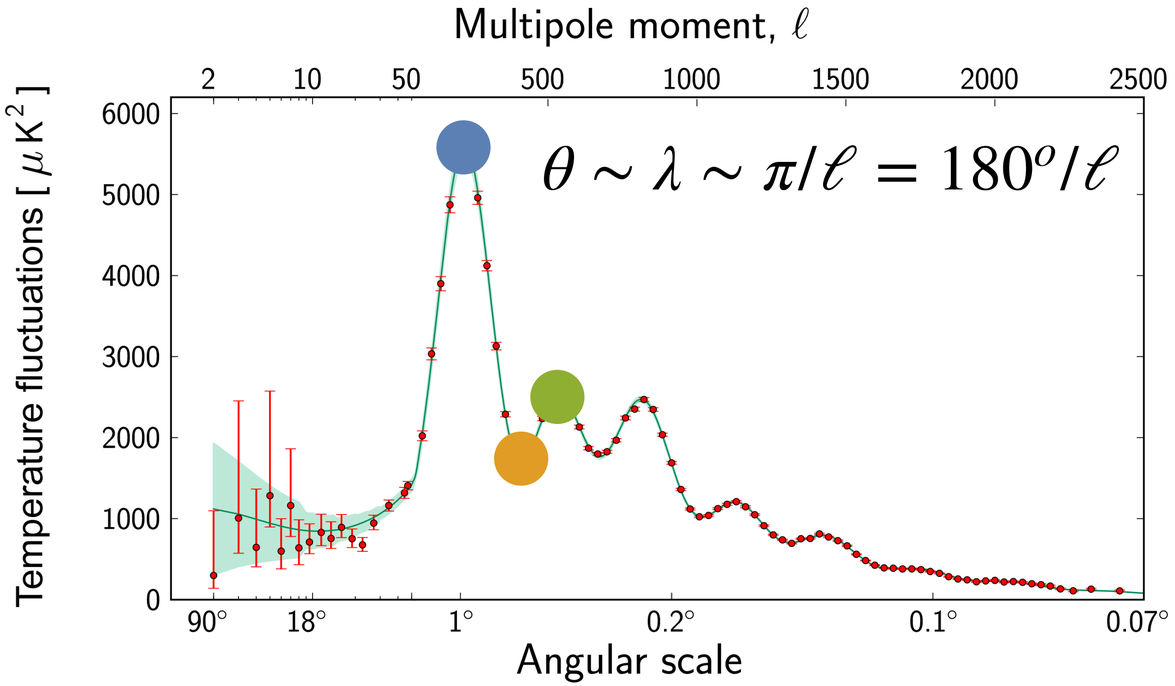

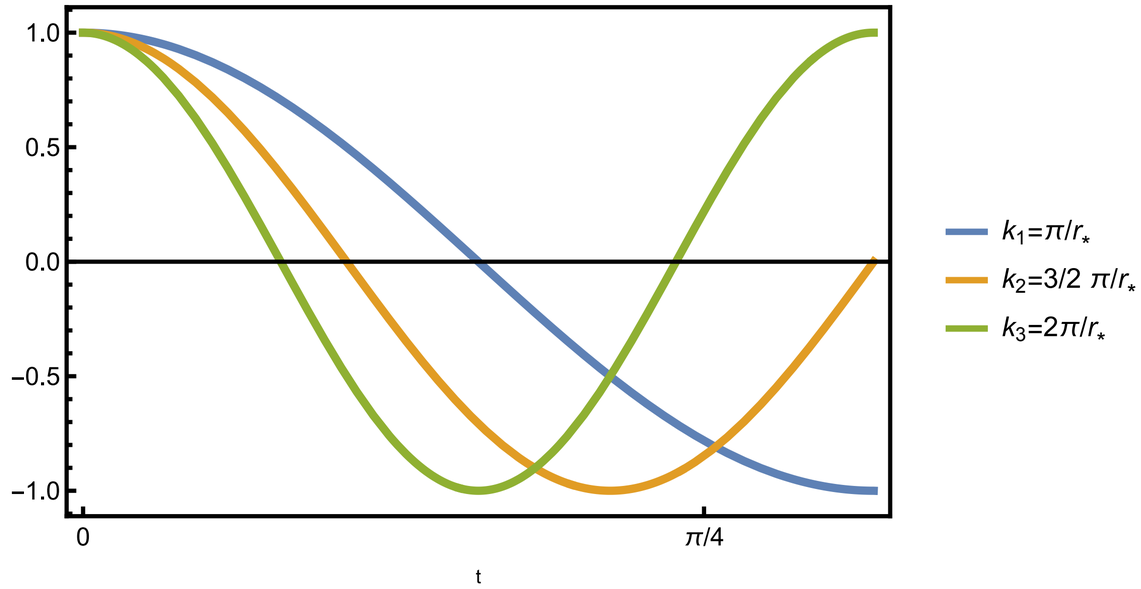

$$\frac{\ell\left(\ell+1\right)}{2\pi}C_\ell^S \sim \frac{A_s}{25}\cos^2\left(\frac{\ell}{\chi_s}r_*\right)$$

$$T_S\left(k,\eta\right) \propto \cos\left(\frac{k\eta}{\sqrt{3}}\right) = \cos\left(kr_*\frac{\eta}{\eta_*}\right)$$

Acoustic Oscillations

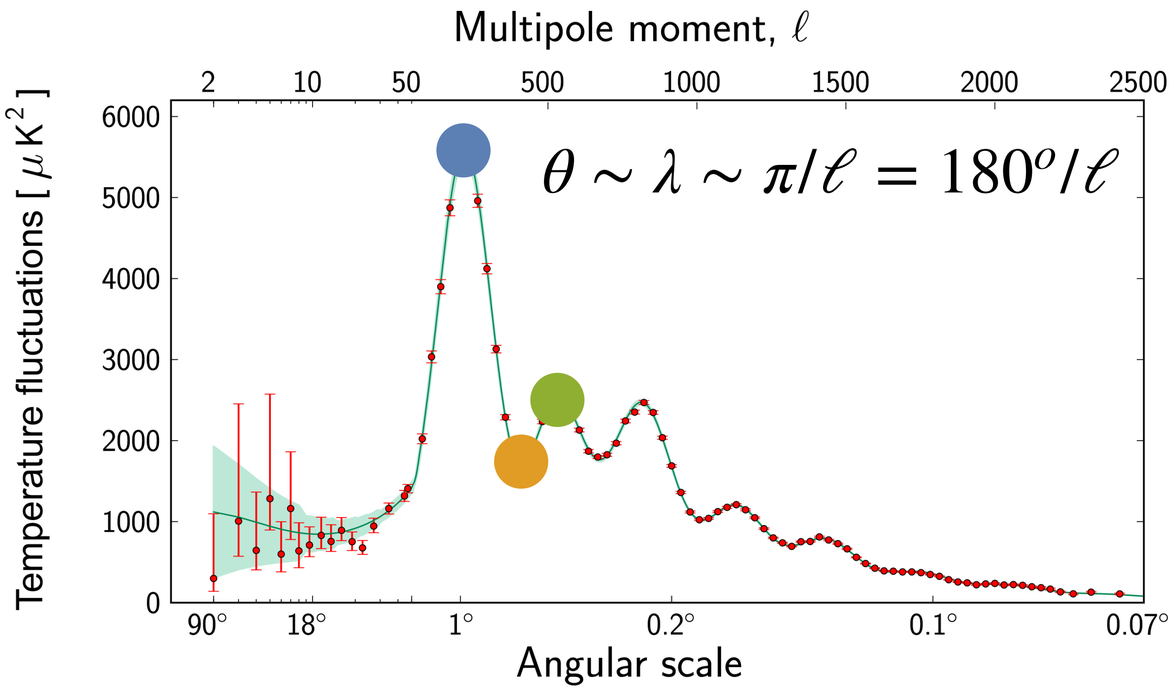

All the modes need to be generated in phase

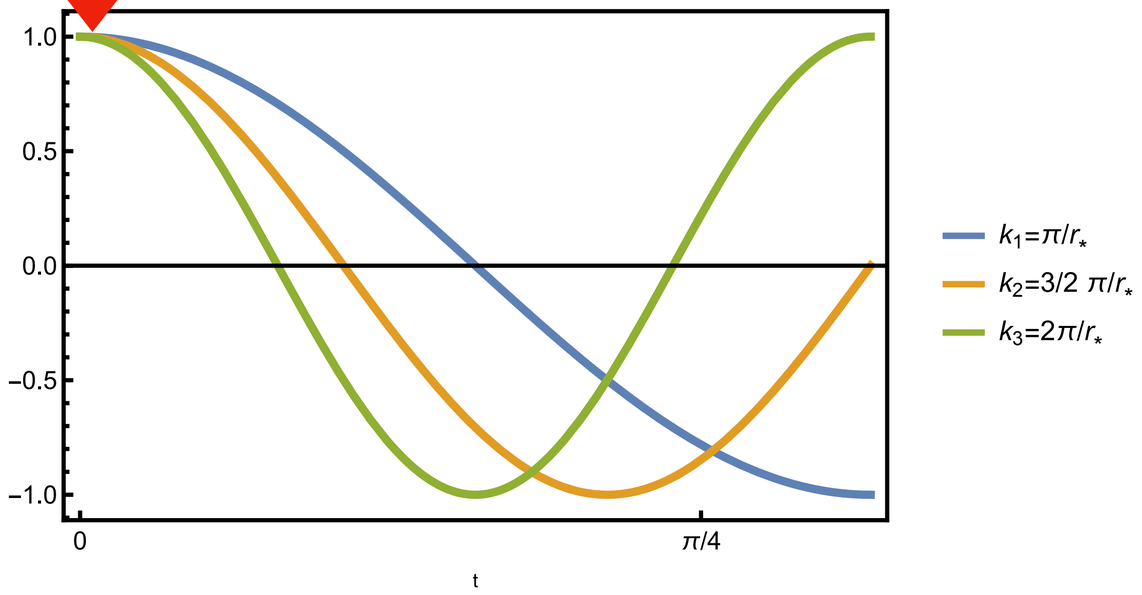

$$\frac{\ell\left(\ell+1\right)}{2\pi}C_\ell^S \sim \frac{A_s}{25}\cos^2\left(\frac{\ell}{\chi_s}r_*\right)$$

$$T_S\left(k,\eta\right) \propto \cos\left(\frac{k\eta}{\sqrt{3}}\right) = \cos\left(kr_*\frac{\eta}{\eta_*}\right)$$

Baryons

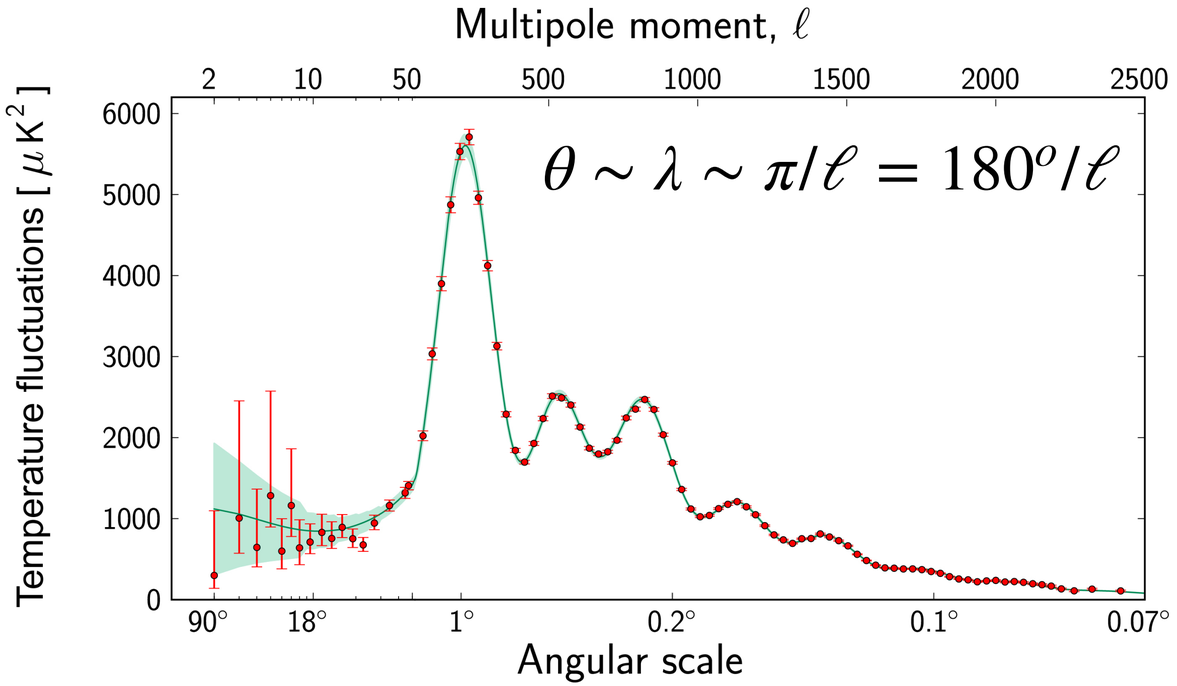

$$T_S\left(k, \eta_*\right) = -\frac{1}{5}\left[(1+3R)\cos(kr_*) - 3R\right]$$

- ☑ flat spectrum at $\ell \ll \chi_*/r_*$
- ☑ peaks at $\frac{\ell}{\chi_*} r_* = n\pi$
- ☑ oscillation not around 0
- ☑ different peaks amplitude
- ☐ absence of first trough at $\ell = \pi/2\ \chi_*/r_*$
- ☐ suppression of power on small scales

Doppler

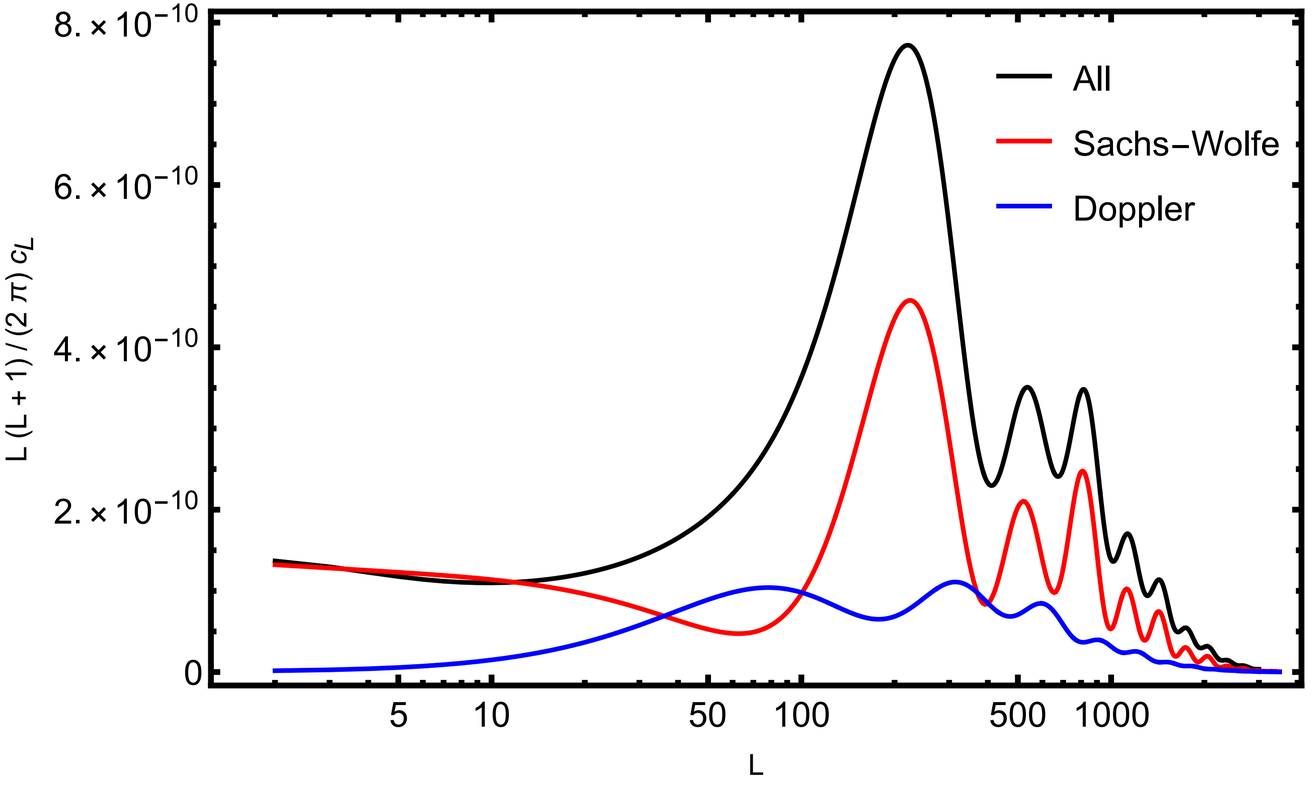

$$T_V\left(k, \eta_*\right) \propto \sin(kr_*)$$

- ☑ flat spectrum at $\ell \ll \chi_*/r_*$
- ☑ peaks at $\dfrac{\ell}{\chi_*} r_* = n\pi$
- ☑ oscillation not around 0
- ☑ different peaks amplitude
- ☑ absence of first trough at $\ell = \pi/2 \ \chi_*/r_*$
- ☐ suppression of power on small scales

Photons Diffusion

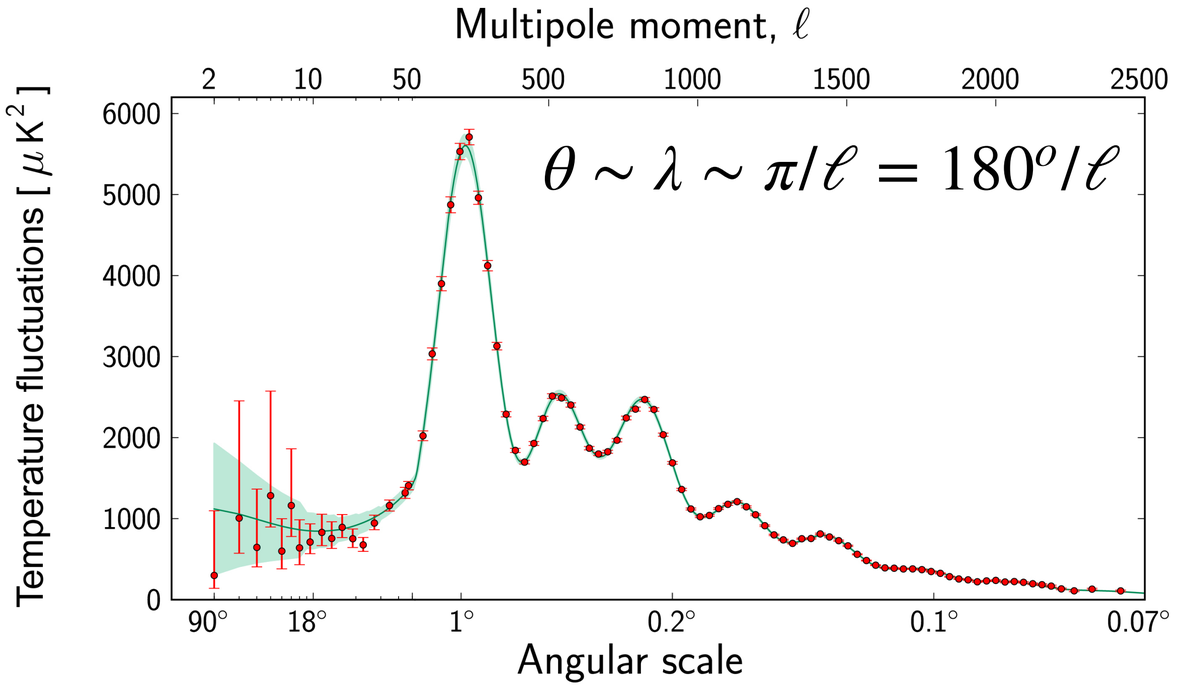

$$\ell_D \sim k_D \chi_* \sim 930$$

- ☑ flat spectrum at $\ell \ll \chi_*/r_*$
- ☑ peaks at $\dfrac{\ell}{\chi_*} r_* = n\pi$
- ☑ oscillation not around 0
- ☑ different peaks amplitude
- ☑ absence of first trough at $\ell = \pi/2 \ \chi_*/r_*$
- ☑ suppression of power on small scales

Cosmological Parameters

Initial Conditions | Matter content | Geometry

A_S n_s Ω_B Ω_M H_0

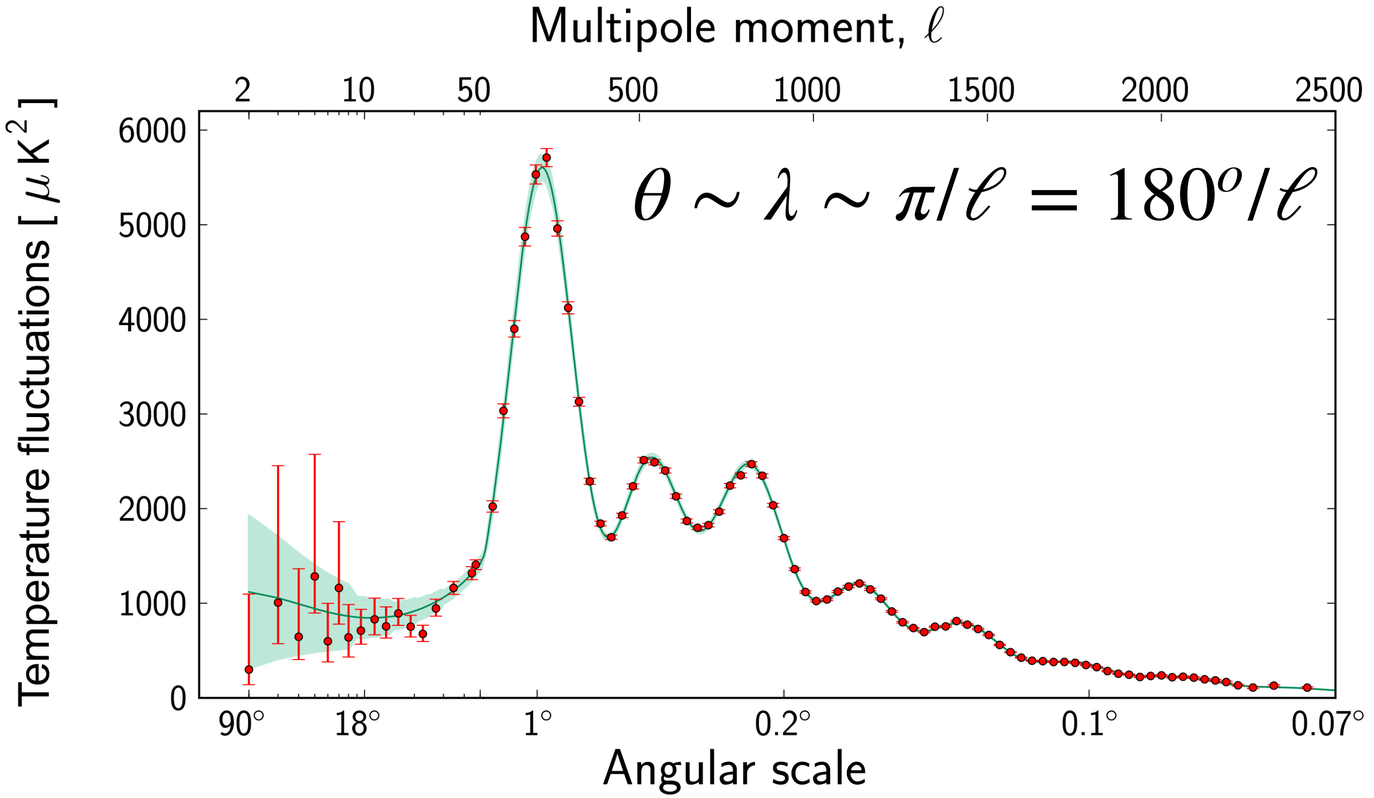

Cosmological Parameters

Initial Conditions | Matter content | Geometry

A_S n_s Ω_B Ω_M H_0

$$P_R = \frac{k^3}{2\pi^2} A_S \left(\frac{k}{k_p}\right)^{n_s - 1}$$

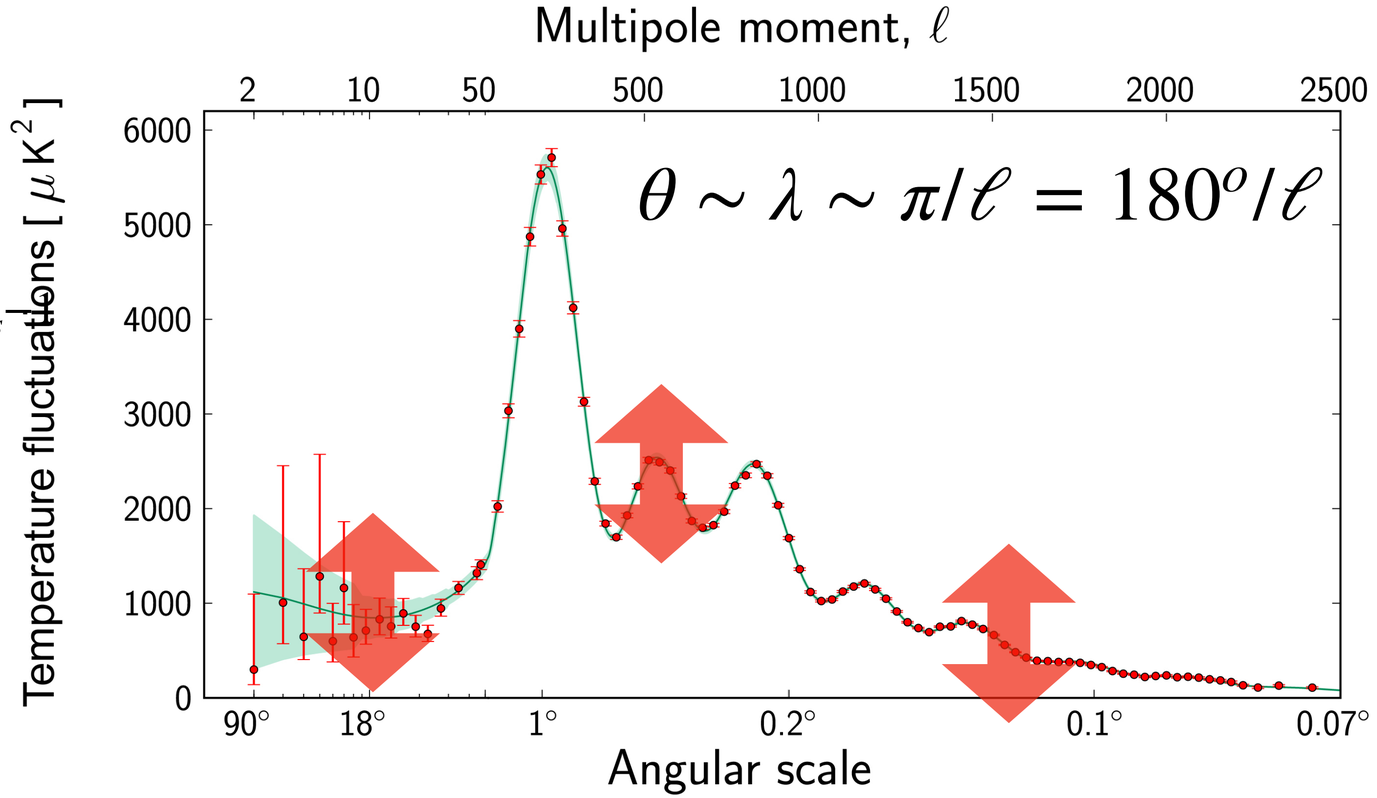

Cosmological Parameters

Initial Conditions | Matter content | Geometry

A_S | n_s | Ω_B | Ω_M | H_0

$$P_R = \frac{k^3}{2\pi^2} A_S \left(\frac{k}{k_p} \right)^{n_s - 1}$$

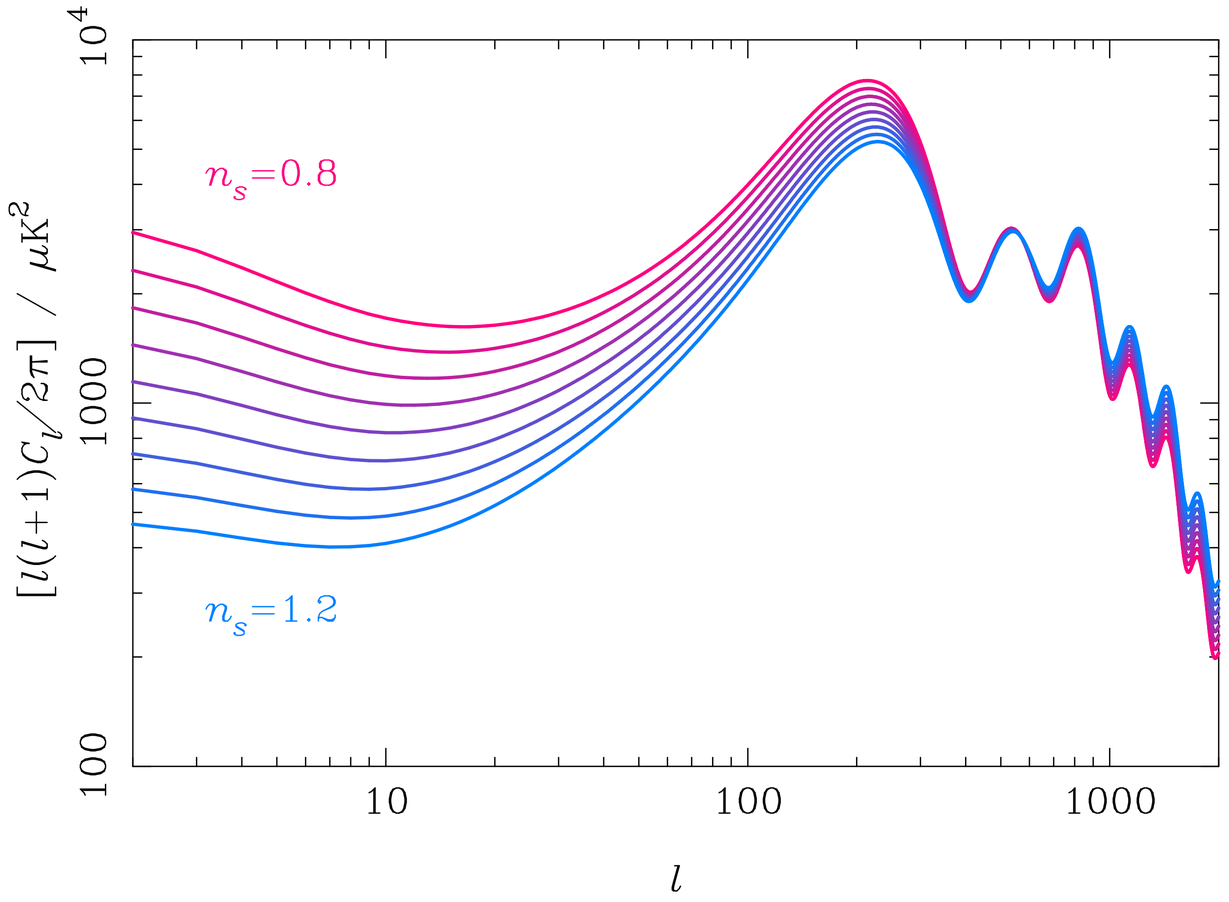

Cosmological Parameters

Initial Conditions | Matter content | Geometry

A_S n_s Ω_B Ω_M H_0

Even vs odd peaks

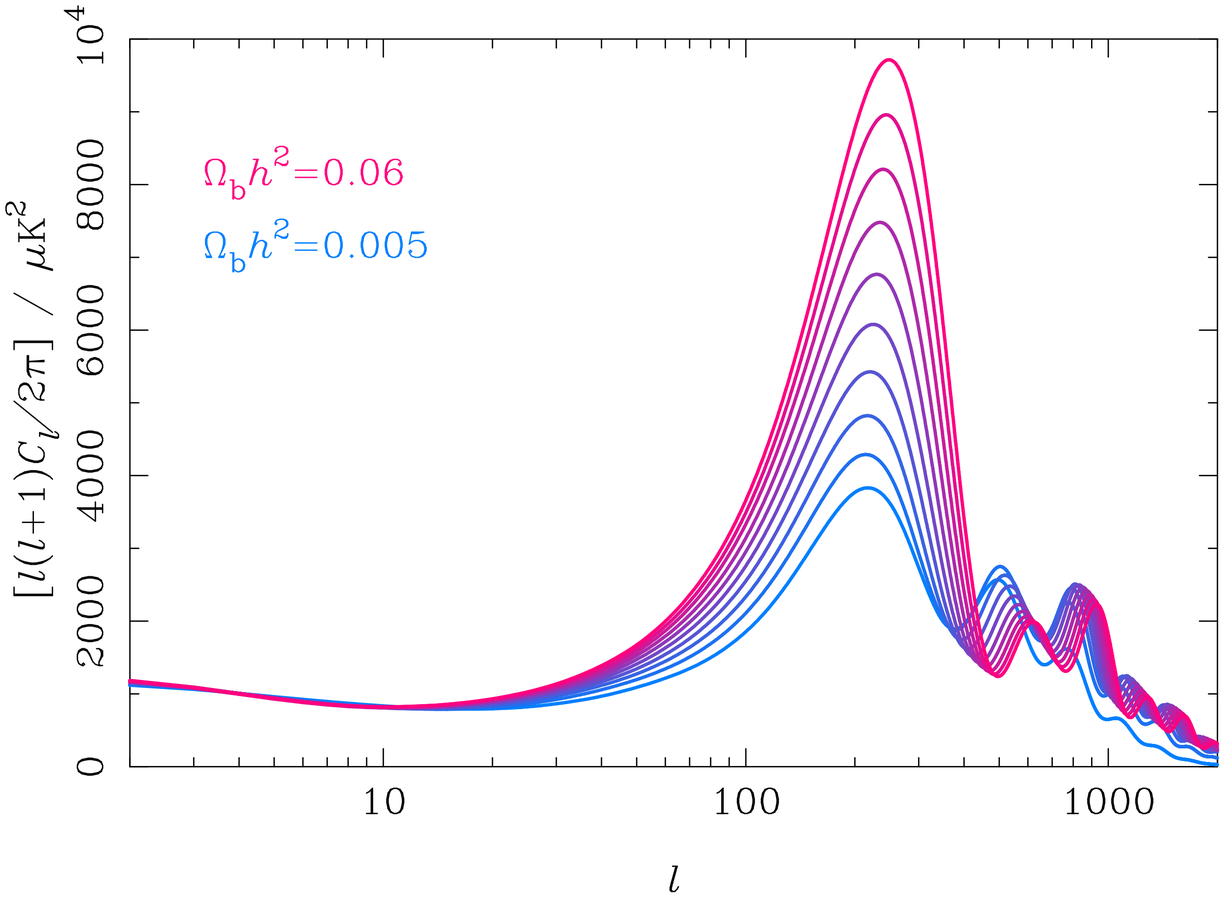

Cosmological Parameters

Initial Conditions | Matter content | Geometry

A_S n_s Ω_B Ω_M H_0

Larger $\Omega_M h^2$

reduces χ_*, r_*, k_D^{-1}

and move $k_{\rm eq}$ to smaller scales

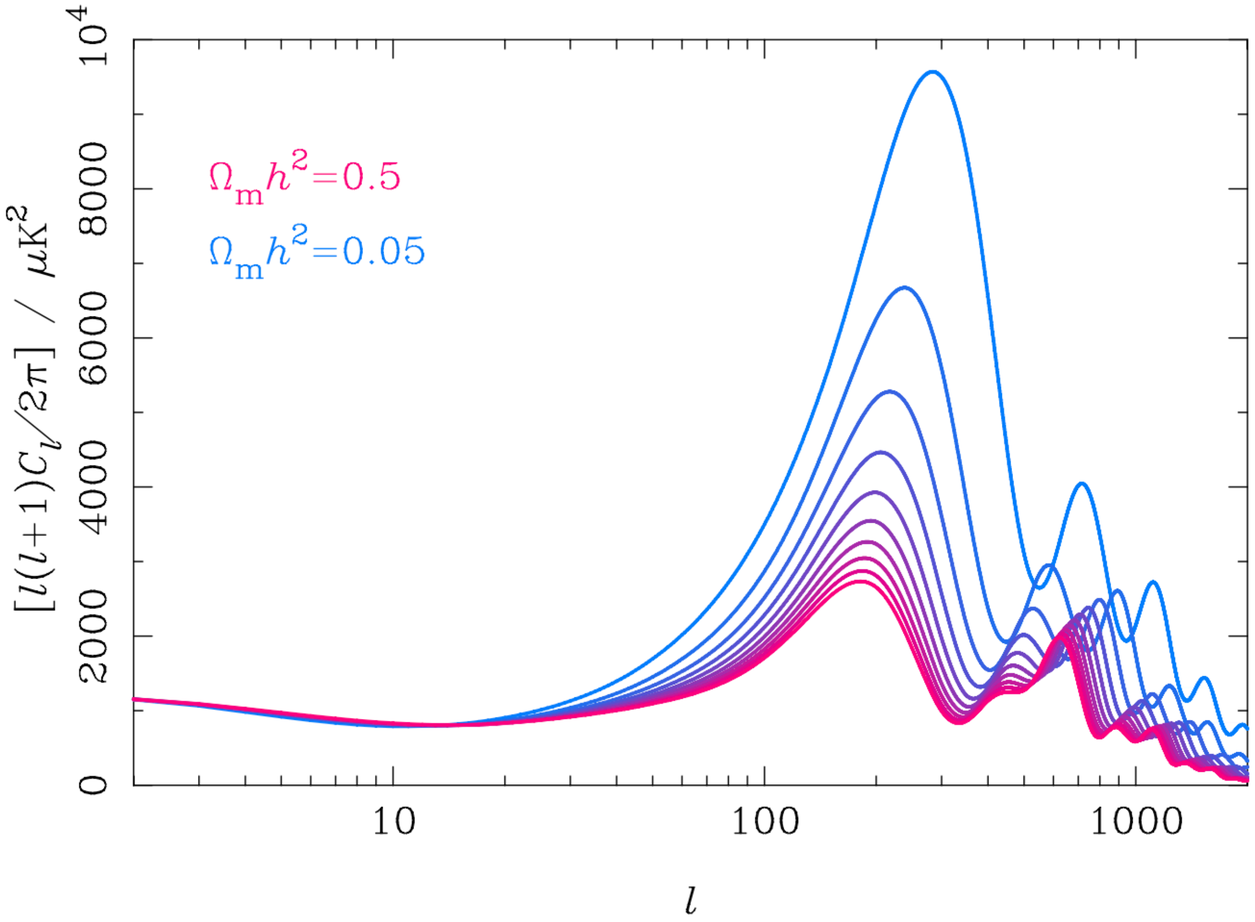

Cosmological Parameters

Initial Conditions

Matter content

Geometry

A_S n_s Ω_B Ω_M H_0

CMB peaks at $\frac{\ell}{\chi_*} r_* = n\pi$

Knowing r_* from the matter content and the primordial plasma physics we have a measurement of χ_*

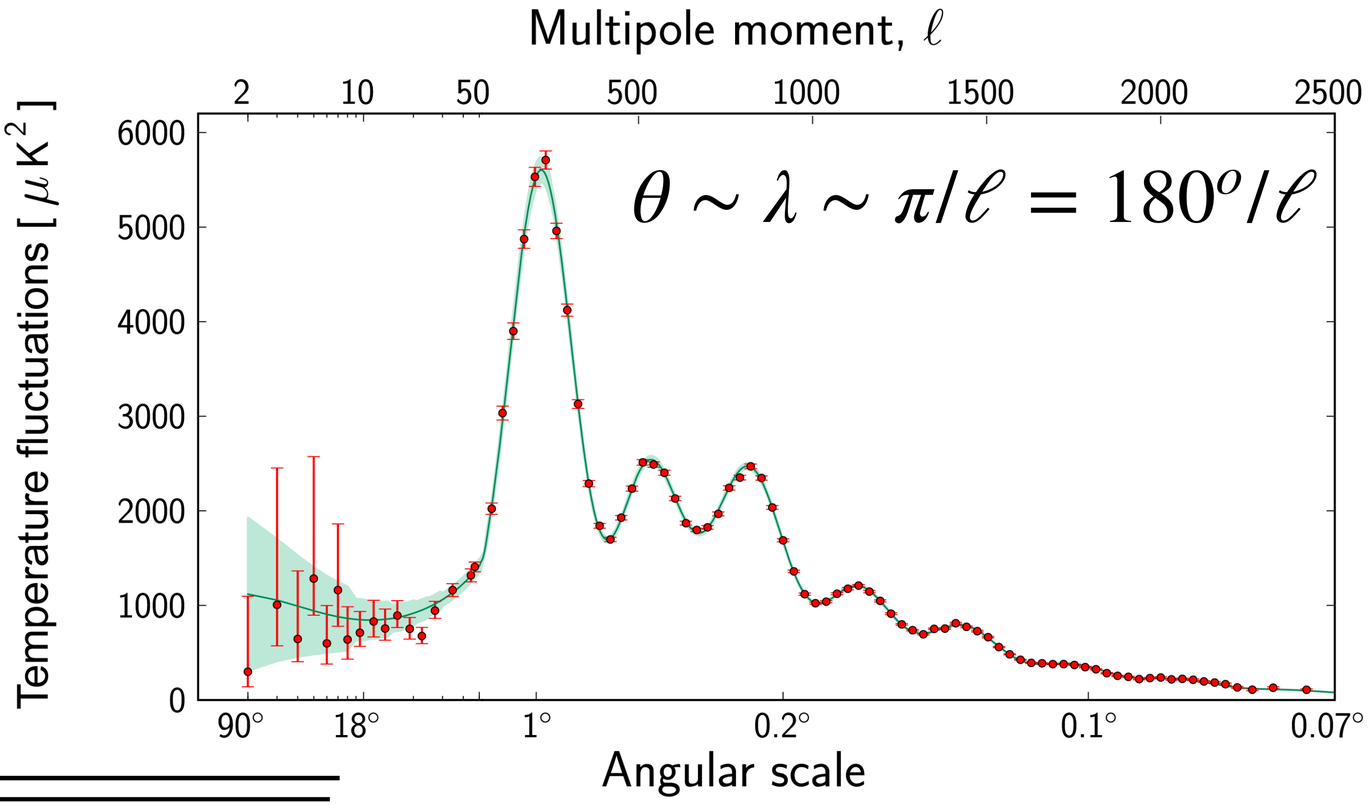

$$\chi_* = H_0^{-1} \int_0^{z_*} \frac{dz}{\sqrt{\Omega_M(1+z)^3 + \Omega_R(1+z)^4 + 1 - \Omega_M}}$$

CMB Degeneracies

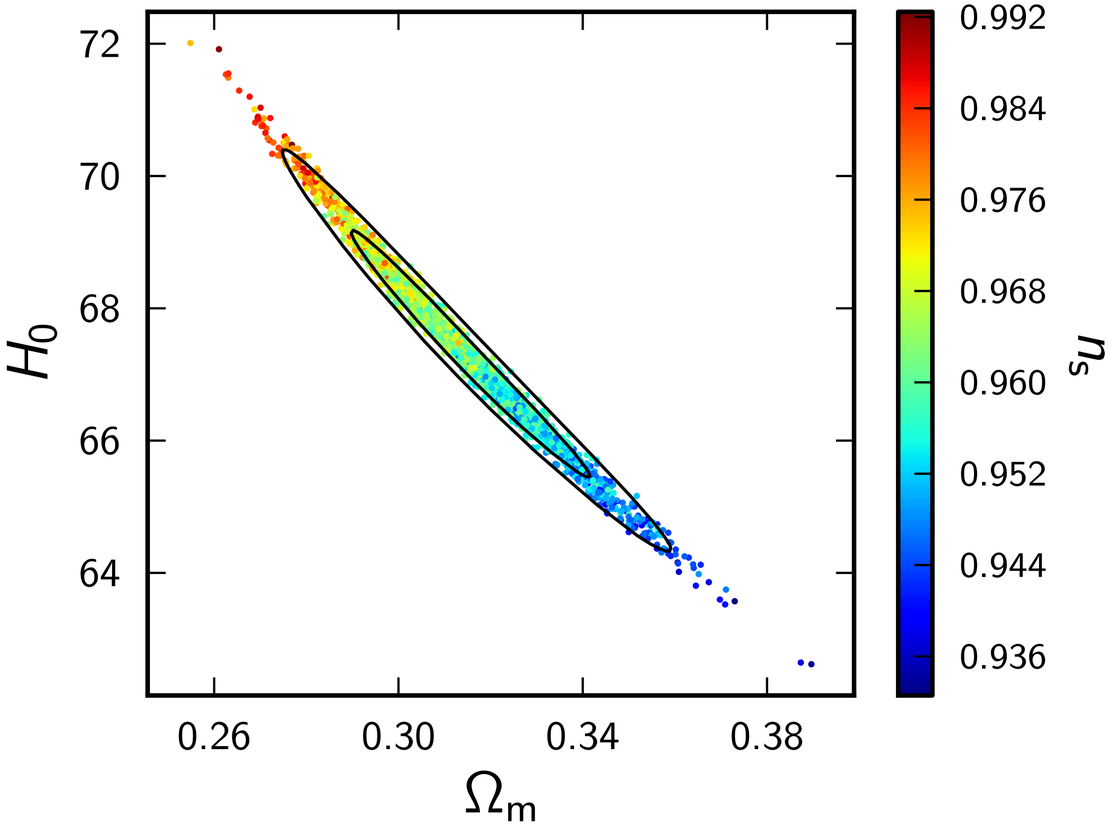

Peaks location very well measured

$\theta_* = r_*/\chi_*(1+z_*)$ measured at $0.05\,\%$

CMB is a very accurate standard ruler

$$\chi_* = H_0^{-1} \int_0^{z_*} \frac{dz}{\sqrt{\Omega_M(1+z)^3 + \Omega_R(1+z)^4 + 1 - \Omega_M}}$$

But many combinations of H_0 and Ω_M can lead to same distance at z_*